

# NANOscientific

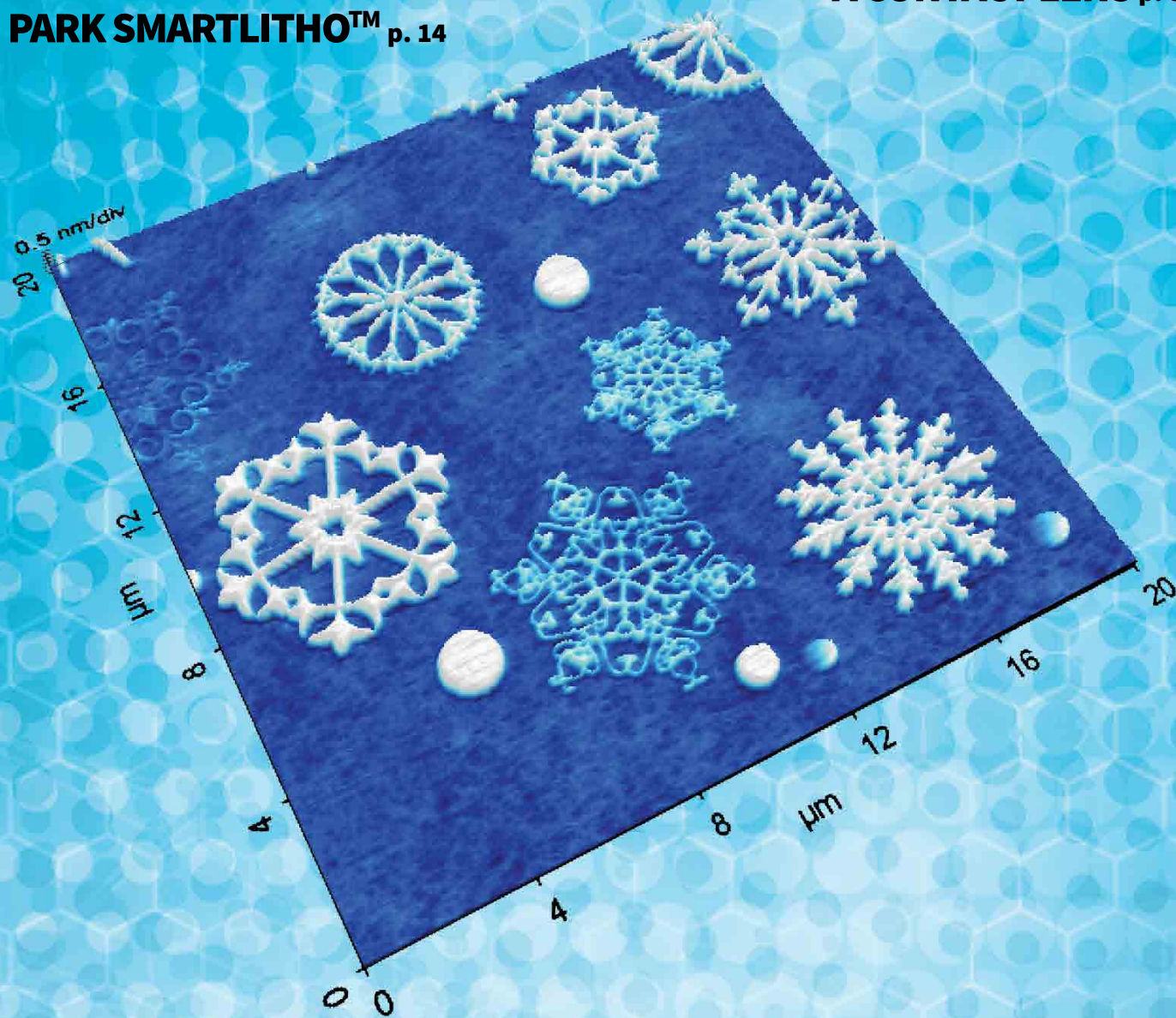
VOL 20 SUMMER 2020

The Magazine for NanoScience and Technology

**CHEMICAL IMAGING IS  
LEADING TO BETTER  
MOLECULAR INFORMATION** p. 5

**CHARACTERIZATION  
OF ROUGHNESS AND  
MECHANICAL PROPERTIES OF  
A CONTACT LENS** p. 8

**PARK SMARTLITHO™** p. 14

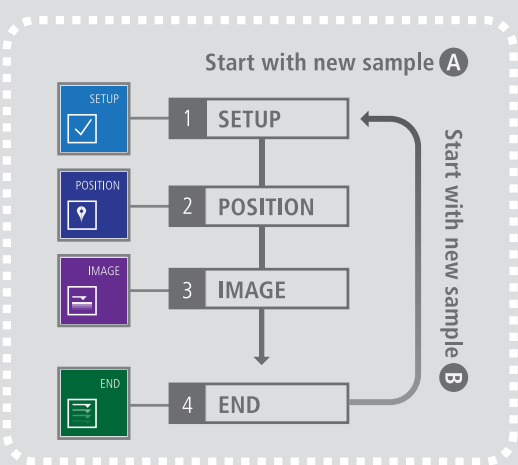


**THE INTERACTION BETWEEN  
LIGHT, MOLECULES, AND  
NANOMATERIALS TO DEVELOP  
SENSORS FOR BIOMEDICAL AND  
OTHER APPLICATIONS USED TO  
COMBAT COVID 19** p. 11



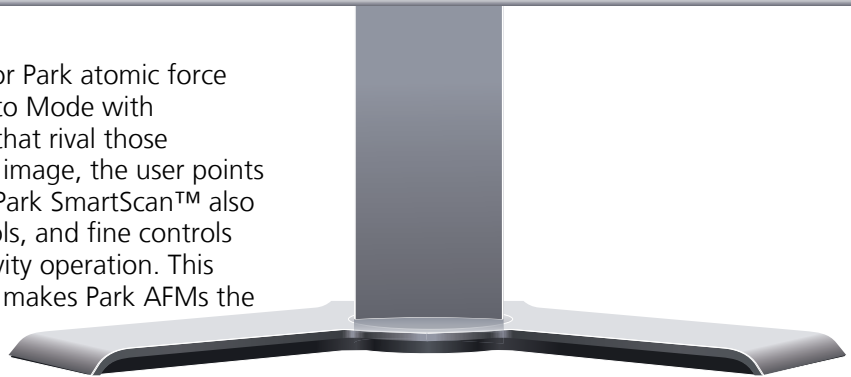
## Park SmartScan™

Bringing the power and versatility of AFM technology to everyone



### Single-Click Imaging with SmartScan Auto Mode

Park SmartScan™ is the revolutionary operation software for Park atomic force microscopes (AFM) that lets inexperienced users scan in Auto Mode with single-click imaging to acquire high quality nanoscale data that rival those obtained manually by experts. Once the user is prepared to image, the user points out a region of interest and a simple click begins the scan. Park SmartScan™ also includes a Manual Mode that provides all the functions, tools, and fine controls seasoned users expect and a Batch Mode for high productivity operation. This combination of extreme versatility, ease-of-use, and quality makes Park AFMs the most powerful atomic force microscopes available.



To learn more about Park SmartScan  
Please visit [parksystems.com/smartscan](http://parksystems.com/smartscan) or email: [inquiry@parksystems.com](mailto:inquiry@parksystems.com)

**Park**  
**SYSTEMS**  
[parksystems.com](http://parksystems.com)

# TABLE OF CONTENTS

NanoScientific Vol 20

## Chemical Imaging is Leading to Better Molecular Information from the Micro to Nanoscale

Rohit Bhargava, PhD, Beckman Institute for Advanced Science and Technology, Cancer Center at Illinois, University of Illinois at Urbana-Champaign

## Characterization of roughness and mechanical properties of a contact lens surface using atomic force microscopy (AFM) with a specialized liquid cell

Research Applications Technology Center, Park Systems Corp.

## The Interaction Between Light, Molecules, and Nanomaterials to Develop Sensors for Biomedical and other Applications Used to Combat Covid 19

Zac Schultz, PhD., Dept. of Chemistry and Biochemistry The Ohio State University

## Park SmartLitho™ – A Novel Approach for Nanopatterning Using AFM Lithography

Research Application Technology Center, Park Systems Corp.

## Park SmartScan and AutoScript: Improving Operational Throughput and User Productivity

Global Technical Marketing, Park Systems Corporation

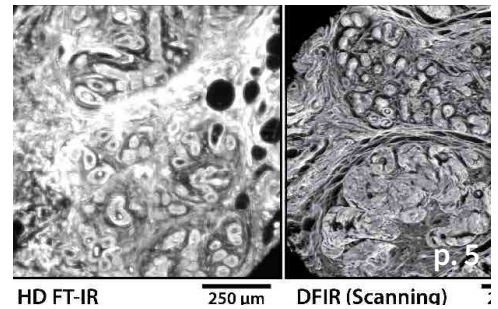
## Nanoscience in GeoScience – Nanopore Characterization Using Atomic Force Microscope

Farzam Javadpour, Ph.D., Bureau of Economic Geology, Jackson School of Geosciences, The University of Texas at Austin

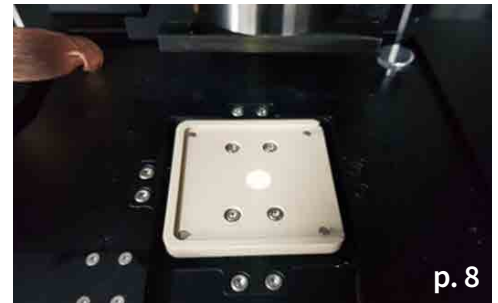
## “Materials Matter” Column 5 - 4D Printing

Dr. Rigoberto Advincula, Professor, Macromolecular Science & Engineering, Case Western Reserve University

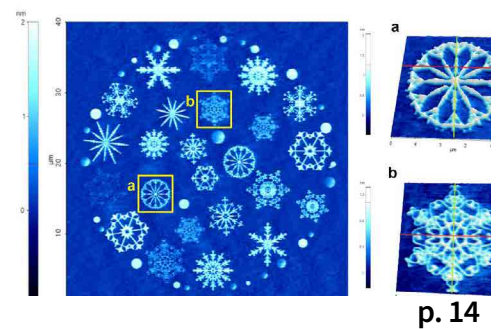
5



8



11



14

19

22

26



## NANOscientific

Keibock Lee, Editor-in-Chief  
kei@nanoscientific.org

Debbie West, Content Editor  
debbiewest@nanoscientific.org

Byong Kim, Technical Director

Debbie Bishop, Art Director

Richard Oettinger, Marketing Manager

Publisher & Corporate Officers  
Park Systems Corporation

Sang-il Park, Chief Executive Officer

Karen Cho, VP of Finance

Keibock Lee, President

Park Systems, Inc.

3040 Olcott Street

Santa Clara, CA 95054

inquiry@parksystems.com

www.parksystems.com

NANOscientific is published quarterly to showcase advancements in the field of nanoscience and technology across a wide range of multidisciplinary areas of research. The publication is offered free to anyone who works in the field of nanotechnology, nanoscience, microscopy and other related fields of study and manufacturing.

We would enjoy hearing from you, our readers. Send your research or story ideas to [debbiewest@nanoscientific.org](mailto:debbiewest@nanoscientific.org)

To view all of our articles, please visit our web site at [www.nanoscientific.org](http://www.nanoscientific.org)

### INSET PHOTO ON COVER:

The AFM topography image reveals that the design of the nanoscale oxide patterns generated by voltage-biased AFM nanolithography using Park NX10 and SmartLitho™ software is various intricate patterns composed of multiple tiny oxide nanostructures with heights ranging from 0.8–1.5 nm.



Park  
SYSTEMS



## Fully Automated AFM solution for OLED, 2D encoder, photomask and more

Gen 8+  
Flat panel display glass

### Park NX-TSH | The automated Atomic Force Microscopy (AFM) system for ultra large and heavy flat panel displays at nanoscale

As the demand for Atomic Force Metrology for larger flat panel displays increases, Park NX-Tip Scan Head overcomes nanometrology challenges for samples over 300mm. The Tip Scanning Head and gantry style air-bearing stage allows Park NX-TSH to accurately image roughness measurement, step height measurement, critical dimension measurement. Learn more about how to get reliable, high resolution AFM images on your large sample size OLEDs, LCDs, photomasks using Park NX-TSH by watching our video at [parksystems.com/tsh/video](http://parksystems.com/tsh/video)



[www.parksystems.com/nx-tsh](http://www.parksystems.com/nx-tsh)

[inquiry@parksystems.com](mailto:inquiry@parksystems.com)



### NANOSCIENTIFIC 2020 EDITORIAL BOARD



**Dr. Rigoberto Advincula**, Professor, Department of Macromolecular Science and Engineering at Case Western Reserve University.



**Dr. Lane Baker**, James L. Jackson Professor of Chemistry Indiana University



**Mr. Phil Kaszuba**, Global Foundries Senior Member of Technical Staff and lead engineer in their Scanning Probe Microscopy (SPM) laboratory.



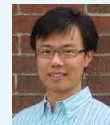
**Dr. John A. Marohn**, Professor & Director of Undergraduate Studies, Department of Chemistry and Chemical Biology Member, Field of Materials Science & Engineering, Cornell University.



**Dr. Ye Tao**, Rowland Fellow & Principle Investigator, Rowland Institute of Science at Harvard University, BA Harvard in Biochemistry, PhD MIT/ETH Zurich Chemistry



**Dr. Gwo-Ching Wang**, Travelstead Institute Chair, Dept. of Physics, Applied Physics & Astronomy, Rensselaer Polytechnic Institute.



**Dr. Jiahua Jack Zhu**, PhD, University of Akron, Associate Professor, Department of Chemical and Biomolecular Engineering.



**Dr. Yiping Zhao** Professor, Department of Physics and Astronomy, Director, Nanoscale Science and Engineering Center, The University of Georgia.

## MESSAGE FROM EDITOR

With the devastating global impact of Covid-19, nanoscale research is propelling us towards a better understanding of ourselves and our relationship to matter. This new issue of NanoScientific covers some of the work happening at nanoscale research facilities worldwide, including new ways to combat Covid-19, innovative technologies to duplicate organs and organisms such as 3D and 4D printing, advanced electronics and artificial intelligence, and efficient energy sources and water remediation. The level of advancement in medical care, for example, has skyrocketed in recent times, where nanobots can even carry medicine through the bloodstream on bacteria cells. We will learn more about that in the next issue and on upcoming NanoScientific TV segments.

Stay tuned for the debut of NanoScientific TV, which will feature segments on nanopore characterization in oil and gas and in medical research,

opening new doors of scientific discovery. We are excited to be able to highlight nanotechnology solutions that are addressing the world's most pressing problems.

This year, our NanoScientific Symposia will be in a virtual format, showcasing researchers who are pioneering medical breakthroughs, novel energy sources, cutting-edge sensors and electronics, and the newest nano topography tools that make all this research possible. Our NanoScientific Symposium for a Changing World is a virtual Ted Talk with a live theatre stage and a program with speakers to engage and entertain the audience. Join our conference and register or submit an abstract or poster at <https://live.parksystems.com/nscw/>

You may also submit your own abstract or PDF poster to present your research at the NanoScientific Symposium for a Changing World. We want to help share your research with our worldwide audience. This year, we will have cash prizes for the best research papers and best poster submissions. Apply now to claim your spot in this exciting event.

**Keibock Lee**  
Editor-in-Chief

For a list of Speakers for  
**NanoScientific Symposium  
for a Changing World**  
visit

<https://live.parksystems.com/nscw/speakers/>

**NanoScientific Symposium**  
Scanning Probe Microscopy (SPM) Applications for a Changing World

**Oct 14-15, 2020**  
[parksystems.com/nscw](https://live.parksystems.com/nscw)

Park Systems presents NanoScientific Symposium hosted by NanoScientific with sponsors Physics World & Nanotechnology World Association

**Park SYSTEMS** **NanoScientific** **NWA** NANOTECHNOLOGY WORLD ASSOCIATION **physicsworld**

# CHEMICAL IMAGING IS LEADING TO BETTER MOLECULAR INFORMATION FROM THE MICRO TO NANOSCALE

Kevin Yeh<sup>1</sup>, Seth Kenkel<sup>1</sup>, and Rohit Bhargava<sup>1,2,3</sup>

<sup>1</sup>Beckman Institute for Advanced Science and Technology

<sup>2</sup>Departments of Bioengineering, Mechanical Science and Engineering, Electrical and Computer Engineering, Chemical and Biomolecular Engineering, and Chemistry

<sup>3</sup>Cancer Center at Illinois, University of Illinois at Urbana-Champaign, Urbana, Illinois, United States

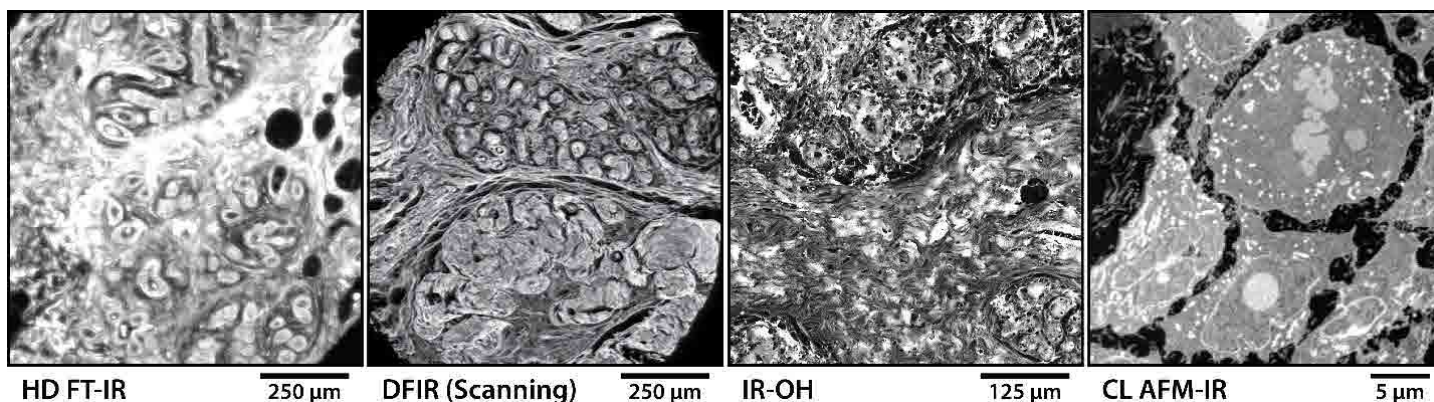


Figure 1. Representative data acquired by CI microscopy systems including: a transmission HD FT-IR system imaging a breast tissue core shown at the Amide I band; a transfection DFIR direct point scanning system also imaging breast tissue when tuned to Amide I; an IR-OH system imaging the PT effect with WF illumination on the Amide II band; and lastly, an AFM-IR system with CL controls imaging at Amide II the protein distribution of subcellular structures within a single cell.

Vibrational infrared (IR) spectroscopy on a spatially resolved microscopic scale, a mainstay of the emerging field of chemical imaging (CI), has seen unprecedented growth in recent years due to the diversity of new instrument designs and measurement techniques. CI expands on our knowledge of traditional microscopy by deriving its contrast intrinsically from the molecular composition of the sample. Across research ranging from medicine to material science, CI has the potential to enable many impactful contributions. For instance, by introducing automatic quantitative processes to pathology or analysis of microplastics via improvements, CI instrumentation are positioned to take advantage of recent revolutions in data science.

Until recently, there have been few realistic options to traditional FT-IR imaging. While modern FT-IR microscopes are an excellent research analytical tool, unsurpassed especially when prior knowledge of the sample is unavailable,

its limitations are apparent for high-throughput routine inspection where we can safely assume a priori information, or for applications where sub-diffraction spatial resolution is necessary. These limitations largely were a result of the low light intensity from globar sources, simply a heated silicon-carbide rod, which was the only option practical for IR imaging. Advances toward higher definition (HD) FT-IR resulted from improved theoretical [1] understanding, but it was not until recent years with broad commercial availability of new quantum cascade lasers (QCL) that turnkey solutions provided a clear path forward. These high-intensity mid-IR sources were combined as multi-laser assemblies that together were tunable across the entire mid-IR fingerprint region. Their narrow-band emission, in conjunction with their discrete single wavelength broad tunability, allowed systems to measure only the precise spectral features of interest, thus enabling high-throughput, discrete frequency infrared (DFIR) spectroscopy.

For targeted applications, the number of discrete spectral bands required for analytics, especially with the recent developments in data science and machine learning (ML), can often be reduced to sufficiently few with limited loss of accuracy. It is often faster to acquire discrete bands sequentially, contrary to the advantage of simultaneous measurement of a wide spectral range as required by a Fourier transform. The most influential spectral features are chosen through careful design, often requiring significant domain expertise, as is the case with most traditional ML techniques. The process of feature extraction and metric definition is often based on prior scientific knowledge and there is a limit on the number of degrees of freedom that can realistically be defined. Thus, by being reliant on the developer, the performance of these older learning algorithms is capped. New deep learning networks require very little human intervention by comparison. Their performance scales by amount

of data and computational power. Especially for biomedical applications, these advances in data science coupled with new CI technology for acquiring vast amounts of information rapidly with cheap computational power and storage, now have the potential to revolutionize diagnostic histopathology and translate CI toward practical clinical use.

The earliest DFIR imaging systems simply retrofitted FT-IR microscopes with a QCL [2, 3]. Over the next several years, several research groups and companies designed new microscopes specifically for integration with QCL sources that specifically take advantage of their many unique properties. The first type of DFIR microscope relies on the direct measurement of residual infrared light after absorption by the sample. These DFIR microscopes have demonstrated drastic improvements in resolution, signal-to-noise ratio (SNR), and imaging speed, thus for the first time, putting CI digital pathology within realistic reach of clinical translation. Systems designed around widefield (WF) laser illumination and utilizing the multi-channel advantage of arrayed detectors have shown exceptional imaging speeds [4]. Meanwhile, scanning systems that tightly focus the coherent laser light into a single spot only a few microns wide [5] and sequentially mapping the sample with high-speed stages, have demonstrated full-slide imaging with unsurpassed spatial and spectral quality at IR diffraction limited resolution [6]. The flexibility of such a platform has also led to expansion of features including simultaneous acquisition of multiple DFs [7] as well as the ability to discern molecular orientations through the measurement of linear dichroism [8].

Recent progress in photothermal (PT) detection provides new opportunities for high resolution CI not possible with conventional IR microscopy. Instead of recording attenuation of IR light, PT instruments encode molecular absorption indirectly by measuring the photo-induced, thermal mechanical response of the sample. Visible Microscopy (VM) and Atomic Force Microscopy (AFM) are the two most common detection methods, both offering resolution beyond the IR diffraction limit. Most notably, VM has shown potential for integrating CI into modern optical microscopy prevalent

in clinical and research workflows for histopathology, an IR-optical hybrid (IR-OH) approach [9], achieving resolution at the sub-micron scale. Similarly, when coupled with AFM scanners, PT detection extends CI to the nanoscale, enabling the study of subcellular molecular chemical structures at high resolution for the first time.

Despite the apparent benefits in resolution, understanding of the processes involved in image formation is limited, resulting in uncertainty in the recorded data. Consequently, these techniques have been reserved for experts whose experience is vital for designing experiments with tightly controlled conditions to mitigate artifacts. Although this approach has seen some success, the applications are obviously limited. Improving PT instruments guided by understanding of image formation offers an alternative to this approach. For example, theory-driven design has led to recent advancements in AFM-based IR (AFM-IR) spectroscopic imaging instruments. To first approximation, the deflection signal of conventional AFM-IR is proportional to the IR absorption near the probe tip; however, the AFM cantilever introduces additional signal correlated to local mechanical properties of the sample. Guided by rigorous analytical modeling of the cantilever, better AFM-IR instruments have been designed incorporating additional measurements [10] and advanced controls [11] to not only correct this effect but also improve the noise of the recorded signal by a factor of five. Each innovation enables new possibilities for CI at the nanoscale such as accurate compositional mapping of biological samples [12]; however more theoretical progress is required to further the limits of detection. Although PT detection is useful for measuring nanoscale molecular information, understanding the image formation is essential for navigating the complex physics governing the recorded signal.

With the extent of progress across theoretical understanding, instrument design, and data analytics, CI is heading to better data for a multitude of new applications, from the microscale to the nanoscale, that have not been previously feasible. Representative data from state-of-the-art CI microscopy systems, as shown in Figure 1, demonstrate a new scope of

biomedical experiments addressable by these modern capabilities. Nevertheless, each of these systems offer unique potential. Systems based on measurement of IR light will be faster simply due to the lack of measurement overhead where each essentially instantaneous detector measurement, sometimes from a single laser shot, can directly map to a single pixel on the image. However, due to the longer wavelength of IR light, these systems are also IR diffraction limited at best and may not sufficiently resolve fine morphologic features. On the other hand, the techniques that rely on a photo-induced sample response can offer substantially higher resolution, in many cases, depending on the resolution limit of the probe instead of the IR beam. Since substantially higher laser power is required to generate a measurable deformation, this restricts possible area of IR illumination typically requiring focused single-point excitation, while also often relying on lock-in amplification or interferometry. Therefore, these techniques are much slower due to the quantity of raw measurements required and its subsequent computation in order to generate each data point. It is important to understand the properties and trade-offs of these techniques and to choose appropriately based on the intended application. The diversity of capabilities provided by this new generation of CI microscopy systems presents scientists with tools appropriate for extracting new information from samples for a broad range of investigations at all length scales.

(1) Reddy, R. R. K. R.; Walsh, M. M. J. M.; Schulmerich, M. V.; Carney, P. S.; Bhargava, R. High-Definition Infrared Spectroscopic Imaging. *Appl. Spectrosc.* 2013, 67 (1), 93–105.

(2) Kole, M. R.; Reddy, R. K.; Schulmerich, M. V.; Gelber, M. K.; Bhargava, R. Discrete Frequency Infrared Microspectroscopy and Imaging with a Tunable Quantum Cascade Laser. *Anal. Chem.* 2012, 84 (23), 10366–10372.

(3) Yeh, K.; Schulmerich, M.; Bhargava, R. Mid-Infrared Microspectroscopic Imaging with a Quantum Cascade Laser. In *SPIE*; Drury, M. A., Crocombe, R. A., Eds.; 2013; Vol. 8726, p 87260E.

(4) Yeh, K.; Kenkel, S.; Liu, J.-N. J.-N.; Bhargava, R. Fast Infrared Chemical Imaging with a Quantum Cascade Laser. *Anal. Chem.* 2015, 87 (1), 485–493.

(5) Yeh, K.; Bhargava, R. Discrete Frequency Infrared Imaging Using Quantum Cascade Lasers for Biological Tissue Analysis. In *SPIE*; Mahadevan-Jansen, A., Petrich, W., Eds.; 2016; Vol. 9074, p 970406.

(6) Mittal, S.; Yeh, K.; Suzanne Leslie, L.; Kenkel, S.; Kajdacsy-Balla, A.; Bhargava, R.; Leslie, L. S.; Kenkel, S.; Kajdacsy-Balla, A.; Bhargava, R. Simultaneous Cancer and Tumor Microenvironment Subtyping Using Confocal Infrared Microscopy for All-Digital Molecular Histopathology. *Proc. Natl. Acad. Sci.* 2018, 115 (25), E5651–E5660.

(7) Yeh, K.; Lee, D.; Bhargava, R. Multicolor Discrete Frequency Infrared Spectroscopic Imaging. *Anal. Chem.* 2019, 91 (3), 2177–2185.

(8) Phal, Y.; Yeh, K. L.; Bhargava, R. Polarimetric Infrared Spectroscopic Imaging Using Quantum Cascade Lasers. In *Advanced Chemical Microscopy for Life Science and Translational Medicine*; Simpson, G. J., Cheng, J.-X., Min, W., Eds.; SPIE, 2020; Vol. 1125210, p 34.

(9) Schnell, M.; Mittal, S.; Falahkheirkhah, K.; Mittal, A.; Yeh, K.; Kenkel, S.; Kajdacsy-Balla, A.; Carney, P. S.; Bhargava, R. All-Digital Histopathology by Infrared-Optical Hybrid Microscopy. *Proc. Natl. Acad. Sci.* 2020, 117 (7), 3388–3396.

(10) Kenkel, S.; Mittal, A.; Mittal, S.; Bhargava, R. Probe-Sample Interaction-Independent Atomic Force Microscopy-Infrared Spectroscopy: Toward Robust Nanoscale Compositional Mapping. *Anal. Chem.* 2018, 90 (15), 8845–8855.

(11) Kenkel, S.; Mittal, S.; Bhargava, R. Closed-Loop Atomic Force Microscopy-Infrared Spectroscopic Imaging for Nanoscale Molecular Characterization. *Nat. Commun.* 2020, 11 (1).

(12) Kenkel, S.; Bhargava, R. Nanoscale Imaging of Biological Samples with Responsivity Corrected Atomic Force Microscopy-Infrared (AFM-IR) Spectroscopy. 2019, No. May, 51.



**Rohit Bhargava** is Founder Professor of Engineering and serves as the Director of the Cancer Center at Illinois of the University of Illinois at Urbana-Champaign.

His primary appointment is in the Department of Bioengineering with joint appointments in several engineering departments and Chemistry as well as in the Carle-Illinois College of Medicine. Rohit graduated with a dual-degree B.Tech. (1996) from the Indian Institute of Technology, New Delhi and received a doctoral degree from Case Western Reserve University (2000). After a stint at the National Institutes of Health, he has been at Illinois as Assistant (2005-2011), Associate (2011-2012) and Full (2012-) Professor. Rohit is widely recognized for his research on chemical imaging and advances in theory, instrumentation, and applications in cancer pathology. Current work in chemical imaging in his laboratory focuses on theoretical modeling that can push the limits of speed and quality of infrared spectroscopic imaging as well as its application in several novel areas. In particular, Rohit's group aims to recognize and subtype cancer by its underlying molecular characteristics, by advanced chemical imaging and application of modern machine learning, ultimately allowing for better treatment of patients. His innovative teaching and mentoring has been consistently recognized by the success of his students. He conceived of and currently directs of the Tissue Microenvironment training program supported by a T32 grant from the NIH. Rohit has also served to

connect the research community in new and exciting ways to take on basic science and engineering questions that surround cancer. He was the first assistant professor hired into Illinois' Bioengineering Department and played a key role in its development. He proposed and has served for ~10 years to develop the Cancer Center at Illinois - a basic science center at the convergence of high quality technology and engineering and oncology.



**Seth Kenkel** is a Postdoctoral Research Associate in the Chemical Imaging and Structures Laboratory at the University of Illinois at Urbana-Champaign. Seth

earned his B.S. (2010) and M.S. (2012) degrees in Mechanical Engineering from the University of Illinois at Urbana-Champaign. After working for John Deere Dubuque Works (2012-2014), he received a doctoral degree in Mechanical Engineering (2014-2020) from the University of Illinois at Urbana-Champaign and was a Tissue Microenvironment fellow (2016-2018). His work focuses on the development of next-generation infrared spectroscopic imaging techniques guided by theoretical modeling from first principles to enable new chemical imaging capabilities at the micro and nanoscale. In particular, he has developed novel hardware and controls to improve limitations on accuracy and noise in nanoscale chemical imaging techniques enabling numerous applications in materials and life sciences. He received the EAS graduate student award (2019) in recognition of this work. His first principles

design approach drives current progress in the development of novel instruments and algorithms to improve the quality of infrared photothermal imaging for wide adoption by novice users in many scientific disciplines.



**Kevin Yeh** is Postdoctoral Research Associate at the Beckman Institute for Advanced Science and Technology of the University of Illinois at Urbana-Champaign.

Kevin graduated with a bachelor's degree (2009) in Biomedical Engineering from Johns Hopkins University, with a master's degree (2011) in Biomedical Engineering from Cornell University, and received a doctoral degree from the University of Illinois at Urbana-Champaign (2019) in Bioengineering. His work in the Chemical Imaging and Structures Laboratory of Professor Rohit Bhargava focuses on the research and development of laser-based discrete frequency infrared microscopes for spectroscopic microscale chemical imaging. He has led the development efforts for multiple generations of custom-built imaging systems, each time pushing the performance of the instrumentation and demonstrating new benchmarks for resolution, noise, and speed. His current work aims to translate these advances into real-world platforms, accelerating the adoption of state-of-the-art chemical imaging microscopes integrated with modern machine learning, thereby enabling better patient diagnostics in clinical environments as well as driving new research interests in material science, chemistry, and biology.



## Park Systems Announces \$1Million Dollar Nano Research Grant Fund

If you are a researcher at a university or government startup lab you may be eligible for a Park Nano Grant. We started the Park Nano Grant program to support researchers that require atomic force microscopy equipment for their up and coming research.

Visit [www.parksystems.com/grant](http://www.parksystems.com/grant) to apply and learn more.



# CHARACTERIZATION OF ROUGHNESS AND MECHANICAL PROPERTIES OF A CONTACT LENS SURFACE USING ATOMIC FORCE MICROSCOPY (AFM) WITH A SPECIALIZED LIQUID CELL

Research Applications Technology Center, Park Systems Corp.

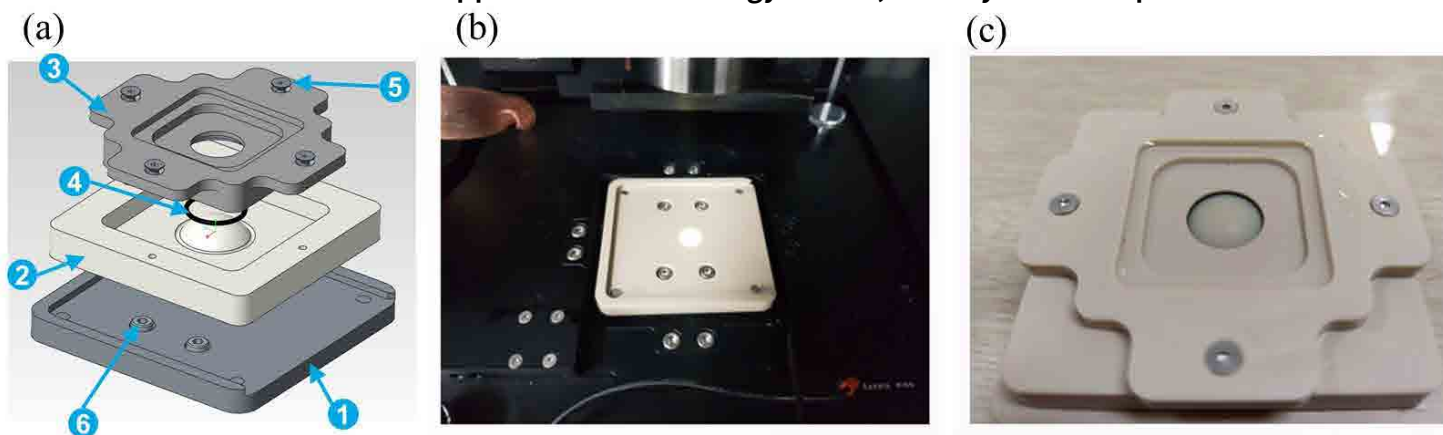


Figure 1. (a) Schematic structure of the liquid cell design for contact lenses, (1) Cell adapter for AFM body (2) Cell Base (3) Cell bracket (4) O-ring between base and bracket (5) 2Φ bolts (6) 2.5Φ bolts; (b) Cell adapter installed on the AFM body; (c) Cell base and bracket components connected with soft contact lens inside.

## Abstract

A soft contact lens is the most utilized type of contact lens, made of gel-type material. This slippery and transparent material, with a unique curvature, like a human eye, requires cutting, drying or freezing to fix for surface characterization. Considering that contact lenses are used in the moist environment inside of human eyes, these preparations result in inaccurate research preparation. The introduction of a liquid cell for contact lenses allows for the placement of a soft contact lens without deformation, and it provides a stable environment for AFM application. In this study, a soft contact lens is fully immersed in saline solution, and its surface, with color coating, is scanned using tapping mode and Park PinPoint™ mode of AFM. The roughness values, Young's modulus, and adhesion energy of the lens surface are successfully acquired with nanoscale resolution using AFM with a liquid cell for the lenses.

## Introduction

As a replacement for glasses, contact lenses are a commonly used for vision correction, providing comfort and convenience. Their use has expanded into

the cosmetic market, and contact lenses are considered as a substitute for invasive surgery. Various studies have focused on the characteristics and material properties of contact lenses, which have led to versatility in properties and application fields [1, 2].

Technical reviews of contact lenses often name surface roughness and material analysis as key factors that define the comfort for users as well as the resistance against bacterial contamination [3, 4, 5]. High-tech manufacturing innovations of the lens mold facilitate lens surfaces with roughness in the nanometer-scale. Lens surfaces take on distinctive roughness and surface adhesion features depending on their manufacturing process and the after treatment [6]. These features establish guidelines for commercial use of contact lenses and lead to innovations in industry research. Among commonly used microscopy techniques, atomic force microscopy is best suited for studying surface properties on the nanometer scale. The capability of AFM at quantitative topography analysis surpasses any other microscopy system – features such as pores or surface defects can be mapped in three dimensions.

Using force distance spectroscopy, AFM additionally obtains mechanical properties like surface adhesion and Young's modulus.

While this versatility is quite useful, the domed shape of a contact lens contrasts with the need for a flat surface for an AFM system to obtain useful surface data. Eventually, lenses are cut or deformed to flatten the surface enough to achieve stable measurement conditions. However, the deformation of the lenses for AFM measurements can entail a loss of information on actual mechanical properties. Here, we introduce a liquid cell for a contact lens measurement. This special cell design has a convex structure with a similar curvature to the human eye to hold a contact lens without deformation. A cover with a hole in the middle fixes the sample and enables access for the AFM tip. We demonstrate surface roughness measurements using tapping mode and Park PinPoint™ Nanomechanical Mode to determine additional properties, such as the difference in Young's modulus and adhesion energy between the center and the color coated layer.

## Materials and Methods

### Liquid cell for contact lens

The cell design consists of three main parts: the cell adapter, the cell base and the cell bracket (bottom to top in Figure 1 (a)). The cell adapter is screwed into the AFM body first (Figure 1 (b)), and then the assembled cell is magnetically attached to the adapter. This configuration allows an independent assembly and manipulation of the liquid cell to facilitate an easy preparation for measurement. A dome shaped support structure on the cell base serves as the mount to affix the contact lens. The curvature radius of the dome is similar to that of a contact lens (~14 mm), so the lens rests on the base without deformation or transformation of its structure. As the collar structure of the cell cover (cell bracket) pushes down the lens, the sample is fixed with its top part open to allow surface access for imaging. In addition, an O-ring is added between bracket and cell base to enhance the stability of sample fixation. The exposed convex top point of the cell base is lower than the cell cover's top surface; this way any contact lens sample can be immersed into saline solution for imaging to simulate real life application.

### Experimental Set-up

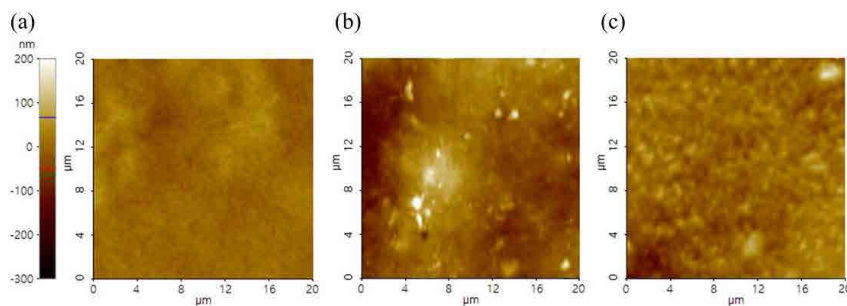
To demonstrate the working principle of the cell, it was mounted to a Park NX12 AFM from Park Systems. We applied saline solution to the cell and fully immersed the contact lens under this solution to maintain the aqueous environment, in which actual usage of the lens mostly occurs. A Biolever Mini (BL-AC40TS) cantilever from Olympus was mounted on the liquid probe hand enabling in-liquid Tapping and PinPoint modes on the soft contact lenses with color coating. The resonant frequency of the cantilever is 110 kHz in air and 25 kHz in water. We chose the Biolever Mini cantilever with a small spring constant ( $k = 0.1 \text{ N/m}$ ) for its softness due to concerns that deformation by the cantilever could change the surface.

### Result and Discussion

Using an optical camera with 10 $\times$  magnification, we examined the sample surface prior to the AFM measurement. The center of this contact lens is transparent and the coating layer covers the rim of the lens as common in colored contact lenses (Figure 2 (a)). Optical images of these two different regions are shown in Figure 2; in the center (b) and on the color coated outer ring (c).

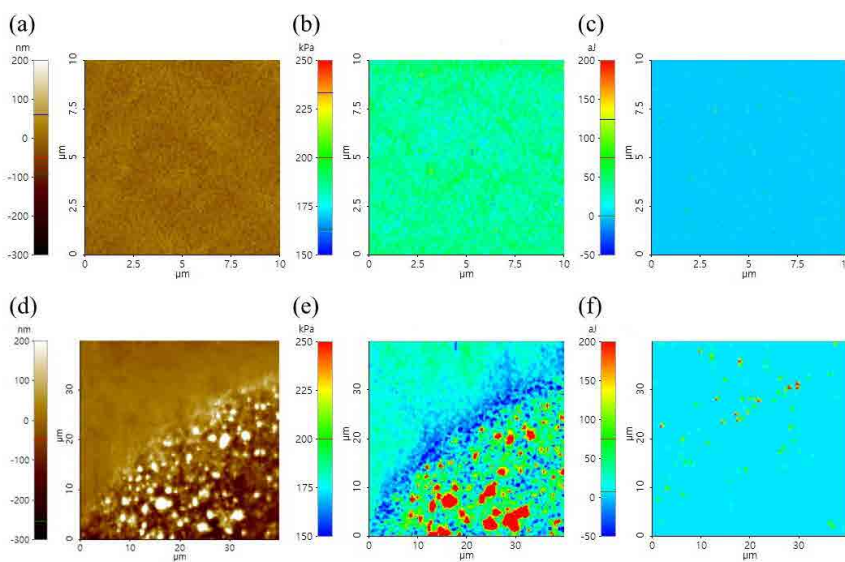


Figure 2. (a) Concept drawing of a soft contact lens with a color layer; (b) Optical camera image: Center of the lens surface on the convex top region; and, (c) color coated area. The red circles mark the AFM scan areas. The optical image scale for both (b) and (c) is  $480 \mu\text{m} \times 360 \mu\text{m}$ .



		Center	Color Dot Edge	Color Dot Inside
Roughness (nm)	$R_{pv}$	132.01	242.56	385.27
	$R_q$	16.52	23.81	46.84
	$R_a$	12.70	18.14	36.81

Figure 3. All images are scaled to the same color. (a) Topography result of the center region on the top of the lens. Topography on the edge (b) and inside (c) of the color dot. (d) Peak to valley ( $R_{pv}$ ), root mean square roughness ( $R_q$ ), and average roughness ( $R_a$ ) chart from (a), (b), and (c).



		Center	Color Dot Edge	Color Dot Inside	
Modulus (kPa)		184.87	180.19	Hard Pigment	288.81
				Soft Matrix	164.03
Adhesion Energy (aJ)		7.32			

Figure 4. Height (a), modulus (b), and adhesion energy images (c) at the center of the lens and at the color dot region (d), (e) and (f), respectively. (g) Modulus and adhesion energy mean values chart; modulus and adhesion energy values in center from (b) and (c), modulus of the edge and inside of color pigment were partially analyzed from (e), and adhesion energy for mean value of the whole image except some high-peaked distinctive points from (f). All images were performed using PinPoint™ Nanomechanical Mode.

Each of the optical images are marked with a red dotted circle where the AFM topography was scanned in the following. For the center region of the lens, we zoomed into the center of the optical position and scanned a  $20\ \mu\text{m} \times 20\ \mu\text{m}$  region (Figure 3 (a)). The same measurements were conducted on both the edge (Figure 3 (b)) and inside (Figure 3 (c)) of the color pigment for comparison. For analysis, three different roughness values were reported: peak to peak difference between the highest and lowest height value (Rpv); root mean square roughness (Rq); and, the average roughness value (Ra).

All three roughness values (Rpv, Rq, and Ra) displayed the same trend, with the smallest roughness values for the center of the lens and the highest roughness in the color pigment, respectively. The color coating increased the surface roughness more than two times compared to the center region, without the coating layer. Furthermore, topography data obtained at the inside of the color pigment showed noticeable differences compared to outside of the color pigment.

For a comparison of the mechanical properties, we scanned the center of the lens and the edge of the coating with the PinPoint technique. While the center region showed homogenous roughness and mechanical property characteristics (Figure 4 (a, b, c)), the edge of the color coating clearly indicated a structural change (Figure 4 (d, e, f)). The coating layer edge was scanned for immediate comparison between the edge (upper left side region) and the inside (bottom right side region) of

the coating (Figure 4 (e)). As the roughness increased towards the color coating, the mechanical properties revealed that this coating consisted of two phases with hard coating pigments embedded in a softer matrix – with respect to the edge of coating, the color pigments were harder and the bottom matrix of the coating was softer.

While the Young's modulus difference is obvious, this feature did not appear in adhesion energy (Figure 4 (e, f)). There were points with high adhesion energy in Figure 4 (f), which were mainly distributed on soft matrix. In these distinctive points, the adhesion energy was 70.48 aJ which was over ten times higher than rest of the image region. Since the tip and sample reaction is acted under saline solution, adhesion energy was not following the regional contrast observed in the modulus image in color pigment images due to the cantilever damping in liquid.

### Conclusions

We introduced a liquid cell with a curvature similar to the structure of the human eye. This cell provided a simple and stable measurement environment for soft contact lenses without deforming or destroying the lens and facilitated imaging in saline solution. Roughness measurements were obtained with a high resolution, comparing the color coated layer with the non-coated substrate. We discovered a clear change in topography as well as the Young's modulus between the two regions of the lens. These results represent the first reference of an AFM study on contact lenses, which can then be used to analyze critical issues such

as degradation and bio-fouling. The new, innovative cell design will allow AFM to become a reliable tool in the contact lens industry, and revolutionize the way contact lenses are studied on the nanoscale.

### References

1. Carnt, N., Wu, Y., & Stapleton, F. (2017) Contact Lenses, Reference Module in Neuroscience and Biobehavioral Psychology.
2. Maulvi, Furqan A., Soni, Tejal G., and Shah, Dinesh O., A review on therapeutic contact lenses for ocular drug delivery. *Drug Delivery*, 23:8 (2016) 3017-3026.
3. Bruinsma, Gerda M., Rustema-Abbing, Minie, de Vries, Joop, Stegenga, Boudewijn, van der Mei, Henny C., van der Linden, Matthijs L., Hooymans, Johanna M. M., and Busscher, Henk J., Influence of Wear and Overwear on Surface Properties of Etafilcon A Contact Lenses and Adhesion of *Pseudomonas Aeruginosa*. *Investigative Ophthalmology & Visual Science*, Vol.43 (2002) 3646-3653.
4. Giraldez, Maria Jesus, and Yebra-Pimentel, Eva, (2012) 'Hydrogel Contact Lenses Surface Roughness and Bacterial Adhesion.' In Adedayo Adio (Ed.) *Ocular Diseases*. London: IntechOpen.
5. Țălu, Ștefan, and Țălu, M., Surface roughness of contact lenses investigated with atomic force microscopy. *The Scientific Bulletin of VALAHIA University – MATERIALS and MECHANICS, Romania*, no. 7 (year 10) (2012) 107-110.
6. Jones, Lyndon, Subbaraman, Lakshman, Rogers, R., and Dumbleton, Kathryn, Surface treatment, wetting and modulus of Silicone hydrogels. *Optician*. 232 (2006) 28-34.

**NanoScientific Symposium**  
Scanning Probe Microscopy (SPM)

**Applications for a Changing World**

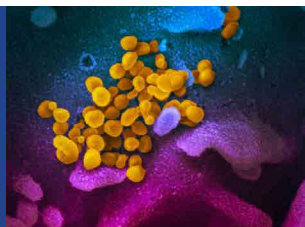
Covers applications in electrochemistry for clean energy, biotechnology for virus and cancer research for saving lives, and other nanomaterial studies for supporting better life.

**Oct 14-15, 2020**  
[parksystems.com/nscw](http://parksystems.com/nscw)

Join us for an Inspiring Symposium that Highlights Nano Applications & Research Leading Towards a Better Future.

Park Systems presents NanoScientific Symposium hosted by NanoScientific with sponsors Physics World & Nanotechnology World Association

**Park SYSTEMS** **NanoScientific** **NANOTECHNOLOGY WORLD ASSOCIATION** **physicsworld**



# AN INTERVIEW WITH PROFESSOR ZAC SCHULTZ

DEPARTMENT OF CHEMISTRY AND BIOCHEMISTRY AT OHIO STATE UNIVERSITY

Prof. Schultz's research focuses on developing innovative approaches utilizing the unique interactions between light and nanostructured materials for near field imaging, ultrasensitive label-free spectroscopic detection, and controlling chemical reactions. His lab studies the interactions between light, molecules, and nanomaterials to develop sensors for biomedical and other applications.

## Can you describe metabolites and explain how studying them can help medical research study disease?

Metabolites are the molecules involved in biochemical reactions that control processes in living systems. They include the molecules that are used to synthesize proteins, produce energy and communicate signals in and between cells. The collection of metabolites in an organism is referred to as its metabolome. While proteins are considered the machines in organisms, the concentrations of different metabolites signify which proteins and biological processes are active, or in the case of disease, are being misregulated. Because the body uses many of the same molecules for different functions, the change in a single metabolite is hard to interpret. It is believed that by monitoring as many metabolites as possible at the same time, one gets a better picture of what is happening biologically speaking.

## Is there any way studying metabolites helps us understand the COVID-19 virus?

Yes, early on the symptoms and treatment for COVID-19 were based on the activated pathways in the body. Metabolites and other biological markers of inflammation were seen to be causing respiratory distress. There have also been reports of neurological effects, which may result from changes in other biological pathways. Metabolomic studies will play a role in understanding the physiological changes that occur with the disease.

## How are metabolites identified and detected?

In metabolomic experiments, the goal is to identify and quantify metabolites. There are more than 40,000 metabolites in the human metabolome. On top that there is evidence that metabolites from the microbiome (bacteria and microorganisms living in our body, like in our digestive tract) also are important in human health. The most common techniques are nuclear magnetic resonance (NMR) and mass spectrometry (MS). MS can detect metabolites at lower concentrations and is probably the most prevalent technique. However, MS experiments typically only detect a few thousand metabolites, perhaps 10% of the known molecules. Additionally, the MS and NMR instruments needed are expensive and found only in shared instrumentation facilities and specialized laboratories. New techniques and methods that can complement existing technologies are active areas of scientific research.

## Why is chemical measurement so crucial for scientific breakthroughs. What is your lab doing in this area currently? Please give some examples that your lab is working on.

Being able to identify the molecules in complex systems, such as biofluids or in living cells, typically requires measuring chemical properties. In my lab, we use Raman scattering, or the inelastic scattering of light, to identify and quantify molecules. When a laser is incident on molecules, it causes the molecules to vibrate. The energy transferred into these vibrations changes the frequency (or color) of light that comes off the molecules. By measuring the frequencies of the Raman scattered light, one obtains information about structure and chemical composition of the molecules. The combination of the frequencies and their intensities detected in the Raman scattering can serve as a molecular fingerprint for detection and characterization. Raman spectroscopy is really cool, but the problem is Raman scattering is a pretty

weak effect. To make Raman detection work at low concentrations, we use plasmonic nanomaterials to enhance the Raman signal. When molecules are close to, essentially on the surface of, nanostructures; the Raman scattering is significantly enhanced sometimes by more than a billion times. This technique is known as surface enhanced Raman scattering (SERS) [1].

Currently in my lab we are investigating how the Raman enhancements from plasmonic structures and nanoparticles can be used as chemical sensors.

In our metabolomics work, we use the Raman enhancements from a nanostructured silver surface [2]. We have developed a surface that has a high density of nanostructures that generates a significant and reproducible SERS signal. The SERS surface we use was developed in our lab about 10 years ago [3]. We then developed a method to use this surface in an online flow detector to monitor the molecules from biological samples eluting from a chromatographic separation [4].

Our flow detector increases the interactions with the surface to generate improved and quantitative detection. Our most recent publication in this area looked at changes in metabolites with cancer, but we also investigating whether this detector can be used for other samples such as virus particles.

In other projects in our lab, we image the enhancement from nanoparticles to generate Raman maps of samples. Using an atomic force microscope (AFM) with a nanoparticle at the tip apex allows us to collect Raman scattering from the tip apex, known as tip enhanced Raman scattering (TERS), adding chemical information to the measured topography. We have used TERS to monitor protein receptors in intact biological cells to understand chemical interactions related to protein recognition [5]. We have also used gold nanoparticles with multiple branches known as nanostars to study drug targeting in cells [6]. Again, the SERS signal from the nanostars provides chemical information about the chemical

environment where the gold nanostar is detected.

We are also interested in developing new chemical sensors based on incorporating plasmonic nanoparticles with other materials. Some of these materials can be used for chemically selective or specific detection assays. Others have improved properties arising from the arrangement of the nanostructures and chemical modifications.

### **How might Atomic Force Microscopes be used to study cells such as in viruses?**

Viruses are small, about 50-100 nm in size, and smaller than the diffraction limit of light, which means you can't see them in an optical microscope. This is a size that is easily imaged using an atomic force microscope (AFM). Viruses were originally visualized using electron microscopes, prior to the invention of the AFM. The AFM has become a powerful tool for visualizing objects in the 1-100 nm size regime. Virus particles on a surface could be imaged by AFM, and differences in virus type may be identifiable by changes in shape. TERS experiments using AFM tips, may be able to further detect chemical differences in the molecules and proteins on the virus surface that may provide targets for therapeutic treatment and diagnostic assays.

### **How is Atomic Force Microscopy used in the characterization of sensors?**

In our lab, we use AFM in a couple ways. The first is in TERS experiments. A nanoparticle on the apex of an AFM tip can be used to increase the Raman scattering from sample, adding chemical discrimination to the surface features measured in AFM. In developing the sensors in our lab, the arrangement, density, and organization of nanoparticles on the surface are important characteristics in sensor performance. We use AFM to measure topography and refine our sensor designs. A real advantage of AFM is the measurement can be done under ambient conditions, or even in solutions, which allows us to characterize our sensors under real life conditions. Changes in the sensor topography are often correlated to changes in performance.

### **What are the newest discoveries in sensors being developed at your lab?**

Our most recent work has been in developing chemically sensitive, but non-specific sensors. What that means is the signal we detect contains chemical information that can identify a specific sample, but many different samples can be investigated. The chemical information in the SERS spectrum arises from the sample, so we have a general-purpose detector. This is important because we can obtain a signal that is specific to a sample without knowing exactly what the sample is. This is incredibly useful when you encounter a new sample or want to detect something that has not been studied before. We are working toward making SERS based sensors quantitative and readily available for identifying new and trace targets in real life samples.

### **How are virus cells such as COVID-19 viewed under microscope?**

As I mentioned in the question about how AFM can be used to study viruses. Virus particles are too small for their shape to be seen in an optical microscope and they require an electron microscope or an AFM to be visualized. Even if the shape cannot be resolved, the Raman scattering from a virus can still be detected in an optical microscope, providing a means to detect their presence without seeing their shape.

### **What do you think medical science will learn from the current pandemic outbreak?**

I think we will learn several things from the current pandemic. Some of the things we may learn have to do with how healthcare is delivered, and outbreaks are monitored. I think one area medical science will advance is in the development of rapid, field deployable sensors. Imagine if every person boarding an airplane could be screened for a virus the way they screen for explosives. Containment and the spread of viruses could be controlled much more readily, preventing an outbreak from reaching the pandemic stage. A real challenge here is detecting something before you know what it is. I hope the sensor development ongoing in my lab can help contribute to this goal.

### **References:**

1. Nguyen Anh, H.; Peters Emily, A.; Schultz Zachary, D., Bioanalytical applications of surface-enhanced Raman spectroscopy: de novo molecular identification. *Reviews in Analytical Chemistry* 2017, 36 (4), 20160037.
2. Xiao, L.; Wang, C.; Dai, C.; Littlepage, L. E.; Li, J.; Schultz, Z. D., Untargeted Tumor Metabolomics with Liquid Chromatography-Surface-

Enhanced Raman Spectroscopy. *Angewandte Chemie* 2020, 59 (9), 3439-3443.

3. Asiala, S. M.; Schultz, Z. D., Characterization of hotspots in a highly enhancing SERS substrate. *Analyst* 2011, 136 (21), 4472-4479.

4. Negri, P.; Jacobs, K. T.; Dada, O. O.; Schultz, Z. D., Ultrasensitive surface-enhanced Raman scattering flow detector using hydrodynamic focusing. *Anal Chem* 2013, 85 (21), 10159-66.

5. Xiao, L.; Bailey, K. A.; Wang, H.; Schultz, Z. D., Probing Membrane Receptor-Ligand Specificity with Surface- and Tip- Enhanced Raman Scattering. *Anal. Chem.* 2017, 89 (17), 9091-9099.

6. Sloan-Dennison, S.; Schultz, Z. D., Label-free plasmonic nanostar probes to illuminate in vitro membrane receptor recognition. *Chemical Science* 2019, 10 (6), 1807-1815.



**Zachary D. Schultz, Ph.D.**, is an associate professor at The Ohio State University. Prof. Schultz earned his B.S. degree from the Ohio State University in 2000 and Ph.D. from the University of Illinois at Urbana-Champaign in 2005. His doctoral studies used infrared-visible sum frequency generation spectroscopy to characterize electrochemical interfaces, work that was recognized with an ACS Division of Analytical Chemistry Graduate Fellowship (2004). Upon completing his Ph.D., he was awarded a National Research Council Postdoctoral Fellowship to conduct research at the National Institute of Standards and Technology (USA) and then as a research fellow at the National Institutes of Health (NIH). His research at NIST and NIH developed vibrational spectroscopy and microscopy methods to study cell membranes. While at the NIH, Dr. Schultz was awarded a NIH Pathway to Independence Award. Dr. Schultz began his independent career as an assistant professor of chemistry and biochemistry at the University of Notre Dame in 2009 and was promoted with tenure to associate professor in 2015. In January of 2018, Prof. Schultz moved his research program to Ohio State. Prof. Schultz was named a Cottrell Scholar in 2013 in recognition of his outstanding teaching and research. Prof. Schultz has served on the Analytical Chemistry Editorial Advisory Board's Features Panel and is currently on the Editorial Advisory board of *Luminescence* (Wiley) and *Analytical Methods* (RSC). In 2019, he was named a Fellow of the American Association for the Advancement of Science (AAAS).

# Park Systems AFM - Highest Resolution, Accuracy and Ease of Use Brilliantly Combined

Park Systems creates the world's most accurate line of nanoscale microscopy and metrology tools for research and industrial applications. Our innovation features, such as True-Non Contact™ mode and cutting-edge automation, set our products apart from the competition and make Park Systems AFMs the easiest to use and most advanced AFMs available.

To find out more, please email us at [inquiry@parksystems.com](mailto:inquiry@parksystems.com) or visit us at [www.parksystems.com](http://www.parksystems.com)

## General AFMs

Park Systems provides a range of popular AFMs for general research and industrial applications. Designed to be extremely versatile while still providing the accuracy and functionality necessary to do high quality work, our line of general AFMs offer researchers and engineers alike the ability to get extremely accurate results quickly and easily.

### Applications:

- Biological Science
- Materials Science
- Failure Analysis
- Semiconductor Analysis
- Hard Disk Media Analysis

### Small sample AFM



#### Park XE7

True research-grade AFM for the practical budget



#### Park NX10

The world's most accurate easy-to-use research AFM



#### Park NX-Hivac

The most advanced high vacuum AFM for failure analysis and sensitive materials research

### Large sample AFM



#### Park XE15

Capable, adaptable, and affordable-the best value large sample AFM



#### Park NX20

Power, versatility, ease of use, brilliantly combined for large sample AFM



#### Park NX20 300mm

The leading automated nanometrology tool for 300 mm wafer measurement and analysis

## Bio and Chemical

Biological research is one of the fastest growing fields of the 20th century. Park AFMs have played critical roles in this sector, giving researchers the tools they need to develop novel insights into the vast and complicated processes and structures of biology.



### Park NX10 SICM

Cutting-edge nanoscale imaging in aqueous environments



### Park NX12-Bio

Three compelling nanoscale microscopies in one innovative platform



### Park NX12

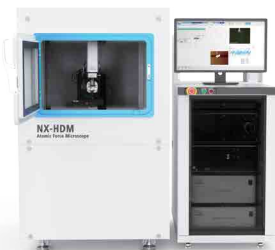
The most versatile AFM for analytical and electrochemistry

## Industrial AFMs

Park Systems is dedicated not just to advancing research, but industry as well. That's why our designers have worked to build a line of the most effective AFMs for FA engineers and industrial applications. Allowing users to take highly accurate measurements and complete their work more quickly, these tools can improve efficiency in the workplace and reduce errors, leading to a more profitable, more consistent development and production process.

### Applications:

- Failure Analysis
- Semiconductor Analysis
- Hard Disk Media Analysis



### Park NX-HDM

The most innovative AFM for automated defect review and surface roughness measurement



### Park NX-PTR

Fully automated AFM for accurate inline metrology of hard disk head sliders



### Park NX-Wafer

Low noise, high throughput atomic force profiler with automatic defect review



### Park NX-3DM

Innovation and efficiency for 3D metrology

## Research Application Technology Center, Park Systems Corp.

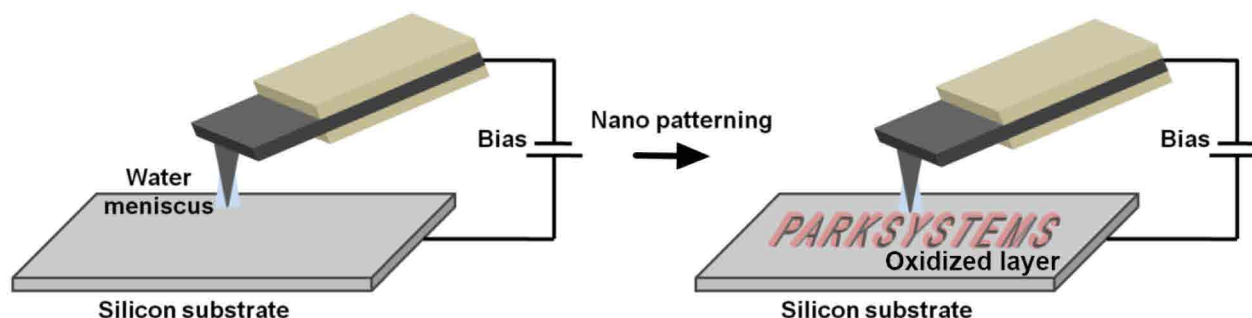


Figure 1. Schematic representation of bias-assisted AFM nanolithography via local surface oxidation. Patterns are created on the surface by oxidation upon bias application between tip and sample.

## Introduction

Since the invention of atomic force microscopy (AFM) [1], it has found widespread application in non-destructive sample surface imaging and significant interest in its electrical, magnetic and mechanical properties. However, in addition to those, AFM offers vast potential for local surface modification and patterning, using either excessive cantilever loading force resulting in mechanical scratching, ferroelectric switching or by oxidizing the surface via the application of AFM tip bias. Local oxidation, also known as ‘bias mode AFM nanolithography,’ has been widely used in the customization of nanoscale conducting or semiconducting surface patterning [2, 3]. Bias mode AFM nanolithography offers many advantages for customized patterning: it circumvents the diffraction limit present in optical lithography methods, it does not require optical masks and its procedure is straight forward. By applying a voltage bias between a conductive AFM tip and a substrate, the tip-sample contact region forms an oxidized layer (Figure 1). Nanopattern control by oxidation occurs by manipulating experimental parameters, including the applied AFM tip bias, the tip material/geometry, scan speed and humidity.

In this application note, we present nanopatterning via oxide growth on a bare Silicon wafer [4] using bias mode AFM nanolithography with Park SmartLitho, the new nanolithography software developed

by Park Systems [5]. Furthermore, we demonstrate the capabilities of Park SmartLitho for lithography on ferroelectric samples by patterning local domains of a PZT (Lead Zirconium Titanate) film on Silicon wafers [6]. Using Park SmartLitho, we fabricated complex structures with detailed and elaborate features, via both oxidation and ferroelectric domain switching.

Finally, we propose optimized process parameters for successful nanopatterning. The software is ideally suited for novel device surface structure development based on nanolithography and for investigations into ever decreasing feature sizes and line spacings for advanced nanoelectronics.

## Materials and Methods

A bare Silicon wafer and a PZT film on a Silicon wafer were used to demonstrate nanopatterning via oxidation and ferroelectric domain switching, respectively. The root mean square roughness ( $R_q$ ) for the bare Silicon wafer was  $> 1$  nm so that the height contrast between the oxidized layer and the substrate could be identified. We used a CDT-NCHR cantilever with a nominal spring constant of 80 N/m and a resonance frequency of 400 kHz for oxidation nanopatterning. The CDT-NCHR tip contains a conductive diamond coating ( $< 10$  kOhm at the Platinum surface) and the tip curvature radius was 100 nm ~ 200 nm. The tip radius of the CDT-NCHR was slightly

larger than tips with other conductive metal coatings; however, diamond coated tips show improved operational stability and higher sensitivity. For nanopatterning via ferroelectric domain switching on a PZT, we used a PPP-EFM cantilever with a nominal spring constant of  $k = 2.8$  N/m and a resonance frequency of 75 kHz.

The PPP-EFM tip has a Platinum-Iridium coating and a radius of approximately 25 nm. Since ferroelectric domain switching on PZT does not require a high loading force between the AFM tip and the sample surface, a soft conductive cantilever was used. The detailed scan parameters are found in Table 1.

All measurements were conducted on a Park NX10 AFM system utilizing Park SmartLitho, the new AFM nanolithography software from Park Systems. Park SmartLitho combines a variety of nanolithography modes, including constant Z scanner mode, constant force mode, bias (and other) modes with a user-friendly graphic editor. The user can access many template types for customized nanopatterning such as bitmap images, polygons, polylines and polydots. Park SmartLitho is available either as a stand-alone version or embedded in the Park SmartScan™ operating software (Figure 2). The stand-alone and embedded versions offer the same functions, like drawing file creation as well as bitmap or pattern editing, and can operate the user’s

## Results and discussion

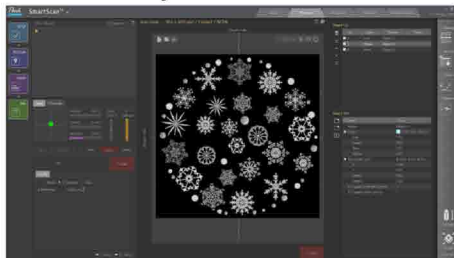
Figure 3 shows the original bitmap image used as the nanopatterning template as well as the height and corresponding 3D images of the sample surface after bias mode AFM nanolithography. The nanopattern on the surface of the bare Silicon wafer resembled the template of the Christmas ball closely. The pattern was generated using bias assisted Silicon oxidation by applying a sufficiently high voltage between the tip and sample. The oxide layer thickness was controlled by the applied bias magnitude and environmental humidity. The oxide layer thickness was directly proportional to the applied tip bias. Furthermore, oxidation required a water meniscus at the AFM tip end that was influenced by environmental humidity [7]. Therefore, the measurement was conducted from a 0 V ~ -10 V tip bias under high humidity conditions (> 60%). The oxide nanopattern featured heights that ranged from 0.8 nm ~ 1.5 nm. Figure 4 shows two of the constituent structures (5  $\mu\text{m} \times 5 \mu\text{m}$ ) with their corresponding 3D images and line profile information. From these line profiles, we confirmed structure heights of approximately 1 nm. The distinct height image contrast after nanolithography illustrated the successful and high-resolution nanopatterning available by bias assisted oxidation using the new Park SmartLitho software from Park Systems.

Figure 5 shows height and Piezoelectric Force Microscopy (PFM) quad images, their line profile information and 3D images after lithography. Ferroelectric domains in PZT can be switched by applying different biases between the tip and sample. We performed both AFM non-contact imaging for height information and PFM imaging for PFM quad information after bias mode AFM nanolithography. As shown in both, the height images were flat surfaces without a pattern. However, the structure resolved in the PFM quad strongly resembled the original traditional Korean pattern template, illustrating successful ferroelectric domain switching. While nanopatterning by oxidation requires humidity control for high-quality nanolithography, nanopatterning via ferroelectric switching requires slow scan speeds and lower loading force scanning to avoid sample damage due to contact mode.

	Nanopatterning by oxidation		Nanopatterning by Ferroelectric domain switching	
Sample	Bare Silicon wafer		PZT on Silicon wafer	
Cantilever	CDT-NCHR		PPP-EFM	
Environment	High humidity (> 60%)		Ambient	
	Nanolithography	AFM image	Nanolithography	AFM image
Scan size	35 $\mu\text{m} \times 35 \mu\text{m}$	40 $\mu\text{m} \times 40 \mu\text{m}$	30 $\mu\text{m} \times 15 \mu\text{m}$	35 $\mu\text{m} \times 25 \mu\text{m}$
Pixel resolution	400 $\times$ 400	1024 $\times$ 1024	300 $\times$ 300	1024 $\times$ 1024
Scan rate	20 $\mu\text{m/s}$	0.5 Hz	10 $\mu\text{m/s}$	0.5 Hz
Bias range	0 ~ -10V	-	0 ~ -10 V	AC bias: 2V DC bias: 0V

Table 1. AFM nanolithography parameters

### a. Embedded system



### b. Standalone system

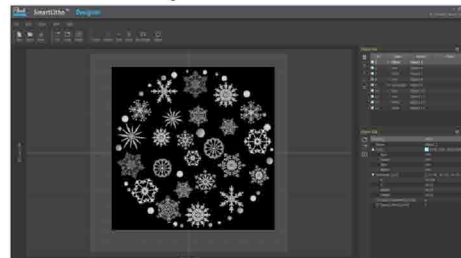


Figure 2. Captured images of Park SmartLitho software, (a) embedded in Park SmartScan imaging software and (b) the stand-alone version.

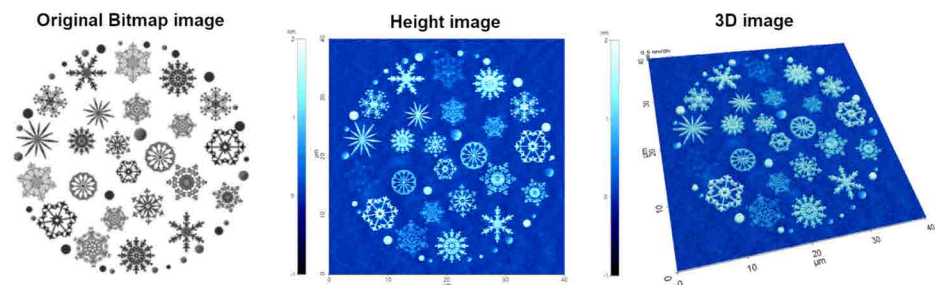


Figure 3. Original bitmap image used as the template (left), AFM height image after bias assisted AFM nanolithography (center) and corresponding 3D image of the sample surface (right). The nanopatterning was generated by surface oxidation.

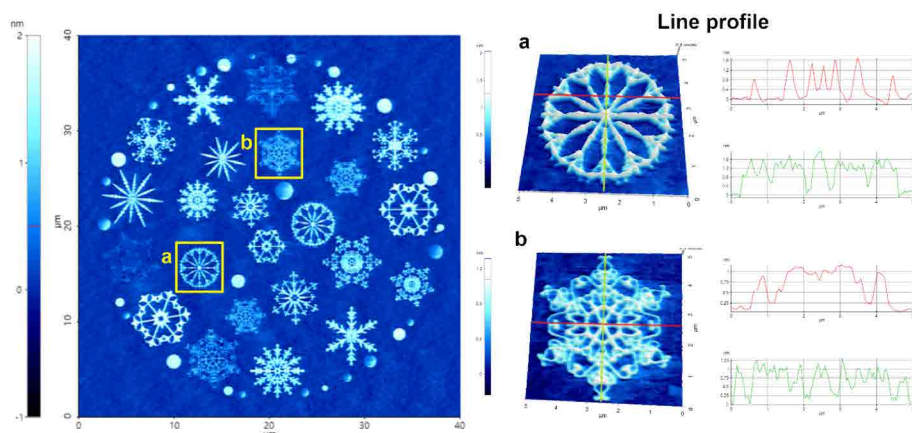


Figure 4. AFM height images after nanolithography and line profile analysis on two of the constituent structures. AFM line profiles in a and b show the ~1 nm height of the oxide layer from the substrate.

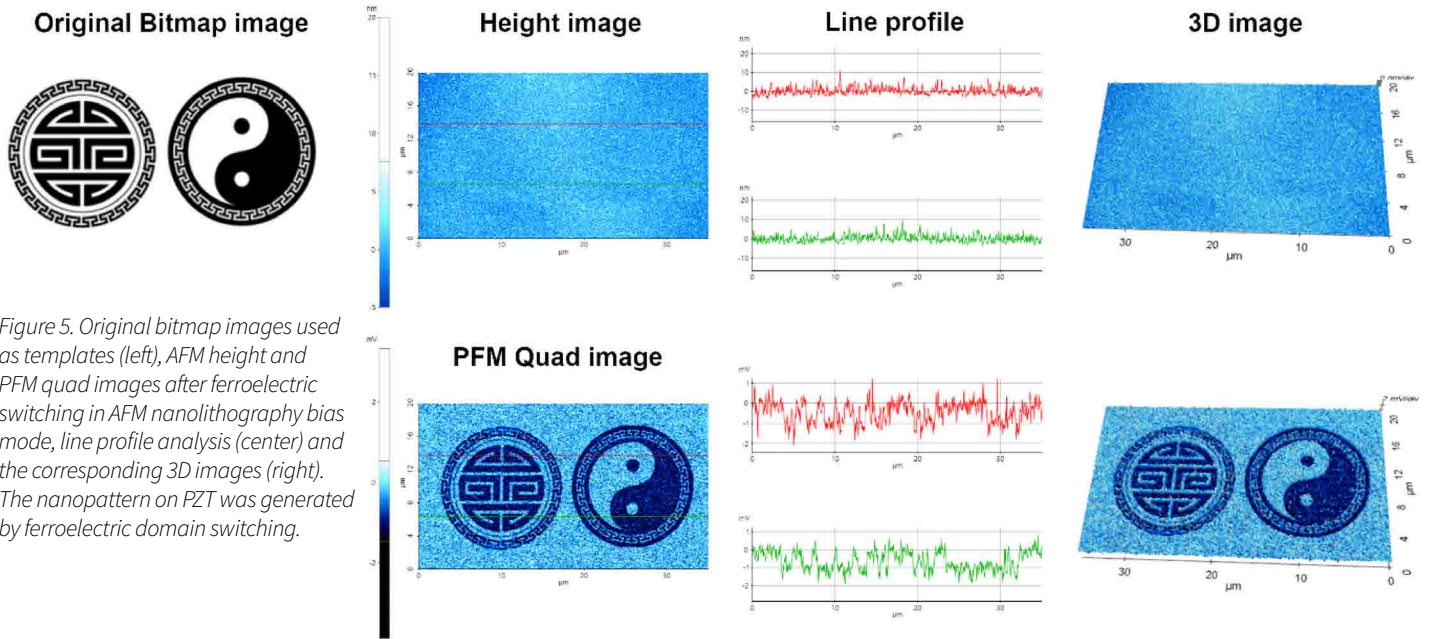


Figure 5. Original bitmap images used as templates (left), AFM height and PFM quad images after ferroelectric switching in AFM nanolithography bias mode, line profile analysis (center) and the corresponding 3D images (right). The nanopattern on PZT was generated by ferroelectric domain switching.

### Conclusion

In this application note, we demonstrate the nanopatterning via oxide growth on a bare Silicon wafer using bias mode AFM nanolithography with Park SmartLitho, a novel nanolithography software from Park Systems on a Park NX10 AFM system. We successfully showed that using Park SmartLitho, a bias assisted nanopatterning of complicated structures can be readily done by locally oxidizing the surface of a Silicon wafer and switching ferroelectric domains of a PZT film. Furthermore, we proposed optimized parameters including humidity values, a tip bias range, scan rate and suitable cantilevers to generate accurate and distinct nanoscale

oxide patterns on a Silicon substrate as well as ferroelectric domain patterns on PZT. This study demonstrates that nanopatterning by AFM nanolithography, in particular oxidation patterning on Silicon substrates and Park SmartLitho, offers significant potential for customized nanosensor surface modification as well as nanodevices for semiconductor research and industry.

### References

1. Binnig, G., Quate, C. F., & Gerber, C., Atomic force microscope. *Physical review letters*, 56 (9) (1986) 930.
2. Minne, S. C., Flueckiger, P., Soh, H. T., & Quate, C. F., Atomic force microscope lithography using amorphous Silicon as a resist and advances in parallel operation. *Journal of Vacuum Science &*

- Technology B: Microelectronics and Nanometer Structures Processing, Measurement, and Phenomena, 13 (3) (1995) 1380-1385.
3. Garcia, R., Martinez, R. V., & Martinez, J., Nanochemistry and scanning probe nanolithographies. *Chemical Society Reviews*, 35 (1) (2006) 29-38.
4. Garcia, R., Calleja, M., & Pérez-Murano, F., Local oxidation of Silicon surfaces by dynamic force microscopy: Nanofabrication and water bridge formation. *Applied Physics Letters*, 72 (18) (1998) 2295-2297.
5. Advanced Vector Nanolithography Using Closed Loop Scan System (2010, Online Article). Retrieved from: <https://parksystems.com/park-spm-modes/97-mechanical-properties/251-nanolithography>
6. Li, D., & Bonnell, D. A., Ferroelectric lithography. *Ceramics International*, 34 (1) (2008) 157-164.
7. Abdullah, A. M., Hutagalung, S. D., & Lockman, Z., Influence of room humidity on the formation of nanoscale Silicon oxide patterned by AFM lithography. *International Journal of Nanoscience*, 9 (04) (2010) 251-255.

## Park SmartLitho™

The next generation nanolithography and nanomanipulation software combining powerful tools with an easy user interface

**The easiest operating system available for nanolithography and nanomanipulation**

Park SmartLitho, enabled by SmartScan is an AFM based platform that performs nanolithography and nanomanipulation on materials, electrical and electronics devices, nanotechnology and other areas of research.

### ATOMIC FORCE MICROSCOPE

For more information send a message to [inquiry@parksystems.com](mailto:inquiry@parksystems.com) or visit [www.parksystems.com](http://www.parksystems.com)



# PARK SMARTSCAN™ AND STEPSCAN AUTOSCRIPT: IMPROVING OPERATIONAL THROUGHPUT

Global Technical Marketing, Park Systems Corporation

## Introduction

Atomic force microscopy (AFM) was originally developed in the 1980s with its first usage in published experimentation taking place in 1986. AFM operation is based on using a cantilever with a sharp probe tip, with an average radius curvature of several nanometers, to scan across a sample surface. The deflections and contortions of the cantilever as its probe tip traces the topography of the sample surface is recorded and then rendered into a computer-generated image for user analysis. Over time, AFM has seen a number of dramatic advances which have enabled it to measure other types of signals from samples not just mechanical feedback. Electrostatic and magnetic forces as well as thermal and electrical conductivity are amongst many quantities now measurable with AFM. Yet despite the advances in the versatility and accuracy of AFM over the years, breakthroughs in improving user throughput have until now historically remained modest in comparison. For example, a common hardware design in many basic AFMs consists of a small sample stage, often manually controlled, that limits the size and number of samples which can be scanned and siphons user attention during tool operation. Boosting the productivity of the AFM user is one of the core principles for AFM innovation guiding instrumentation vendors such as Park Systems. And now, one of Park's next-generation initiatives to vastly improve AFM user output is ready for mass adoption: StepScan autoscript, a software-assisted means for even beginning AFM users to automate tool operation.

StepScan autoscript enables AFM automation by leveraging a

fundamental system design choice, a motorized sample (XY) stage, and a recent landmark advance in AFM operation software, Park SmartScan [1]. The large motorized sample stage on Park AFMs affords them several distinct advantages. First, it allows users to load much larger samples to scan than would be otherwise possible on competing systems. Second, it also allows users to simultaneously load smaller-sized samples for sequential scanning—perfect for investigating sets of samples at a time and reducing tool downtime. Lastly, as it is motorized and controlled with command inputs made in the operation software, the stage no longer has to be manually adjusted by an operator when it comes time to scan a different portion of the sample or a different sample entirely. Park SmartScan further builds upon these advantages by introducing several synergistic features of its own. In the software's Auto mode, a self-optimizing scan parameter algorithm simplifies AFM operation for inexperienced users into a straightforward slider adjustment which trades off between scan quality versus speed. Gone now are the tedious trial-and-error approaches previous generations of AFM users had to endure to get the best results out of their scans. With Auto Mode, scan parameters to produce exemplary AFM images can be logged by the system and exported for use in future scans. This ability to generate and leverage pre-optimized scan parameters is extremely potent and serves as the catalyst which enables StepScan autoscript to be as useful as it is for increasing user throughput.

## Method

Autoscript, along with other enhanced user productivity functions, can be found

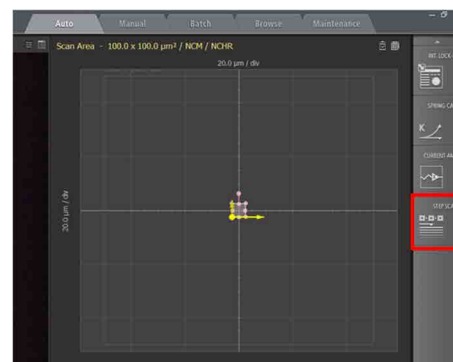


Figure 1. Screenshot of Park SmartScan emphasizing the quick accessibility to advanced functions. Inset red square focuses on the software toggle to activate StepScan autoscript mode.

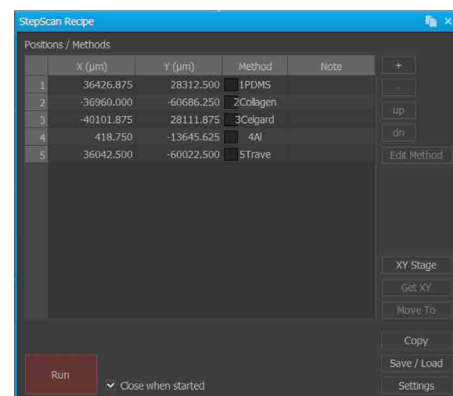


Figure 2. Screenshot of StepScan autoscript's interface for designing a recipe of scripted AFM scans at specific coordinate-based locations on the AFM's sample stage. Note the inset red square which launches a command window for the user to manually control the stage and have the software automatically determine the coordinates for stage's current position.

in another of Park SmartScan's operating modes, Program Mode. As with other similar automation solutions, Autoscript is powered by a series of scripted sample stage movement commands (a recipe) which are interspersed with calls to conduct sample scans using a set of specific parameters (a method). To begin creating a recipe, the user activates Autoscript from within Program Mode (see

Figure 1) and is given a series of blank data fields to fill in using XY coordinates that correlate to specific locations on the sample stage (see Figure 2). These XY coordinates automatically populate the data fields when the user calls up the motorized sample stage's controls from within StepScan and manually guides the stage to a specific location, such as where a sample is currently loaded, underneath the AFM tip. After the XY coordinates for this first scan site have been entered into the recipe, a method can then be assigned in order to define how the imaging should be performed there (see Figure 3). This is particularly compelling for inexperienced AFM operators wishing to automate several scans in sequence—they can take immediate advantage of StepScan autoscript function built into the Park SmartScan to pre-generate optimized methods for them. These two simple steps of defining a recipe's scan locations and assigning a method to each of them is then repeated until all of the desired scans have been scripted. For studies that require larger data sets and more images of the same scan sites, repeating previously scripted steps is as easy as simply copying and pasting multiple row selections as many times as needed. On a Park AFM configured with precision encoders, it is possible to achieve 2  $\mu\text{m}$  repeatability in the XY direction (at 1  $\mu\text{m}$  resolution) and 1  $\mu\text{m}$  repeatability in the Z direction (at 0.1  $\mu\text{m}$  resolution) [2].

Upon executing a recipe finished with Autoscript, the AFM system immediately launches into action and completes all of the user-defined actions without any further operator input. First, the motorized sample stage moves and automatically places itself under the AFM probe tip at the XY coordinates of the first scan. Then, the AFM automatically brings its Z scanner down to have the AFM probe approach the sample. Modern system architecture, such as the one in Park AFM, are both sensitive enough to avoid crashing the Z scanner head onto the sample stage yet quick enough to avoid making the tip approach feel interminable. Once it is in range of the sample, the AFM probe tip engages the sample surface at the scan site and begins scanning using the method assigned in the scripted commands. The AFM probe tip disengages from the sample once the scan at the site is completed. At this point, the

Z scanner will lift back up approximately 10,000  $\mu\text{m}$ .

## Results and Discussion

With a basic understanding of how an Autoscript recipe is set up and executed, we now have sufficient context with which to review scans captured using this function. Five commercial products were chosen for non-contact mode AFM imaging and mounted onto sample holders for simultaneous placement on the AFM's sample stage (see Figure 4). A Park NX20 AFM [3] using a public release build of Park SmartScan featuring Autoscript was used to perform scanning operations on all samples in sequence. High-resolution non-contact mode PPP-NCHR cantilevers from NANOSENSORS [4] featuring a spring constant of 42 N/m and a resonance frequency of 330 kHz were used to image each of the following: (1) a polystyrene low density polyolefin elastomer (PS-LDPE) copolymer standard sample, (2) dehydrated collagen fibrils, (3) celgard, (4) an aluminum triangular production pattern, and (5) a static random-access memory (SRAM) device.

The five samples chosen, together as a set, demonstrate a wide variety of material properties as they range from copolymers, to proteins, to metals, to entire semiconductor devices. Despite the considerable disparity in surface roughness, stiffness values, and nanoscale structures observed in this set of samples, Park SmartScan's Auto Mode was able to successfully conduct survey scans of all samples and log optimized scan parameters for use as methods for insertion into an Autoscript recipe.

### PS-LDPE

Figure 5 shows the optical and AFM topography images of the PS-LDPE copolymer standard sample. This sample is a copolymer of two widely used plastics that have been blended in an attempt to offset one another's material weaknesses [5]. In the AFM image, the darker color represents the PS substrate. The LDPE portion of the sample is represented by the clusters of white scattered through the scan area. Furthermore, the boundaries of each LDPE cluster, as well as several features on top of each of them, are observable in the AFM image.

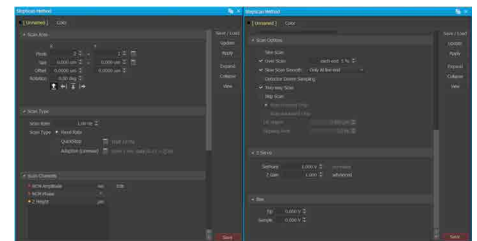


Figure 3. Screenshots of StepScan autocript's interface to implement user-specified methods for one of several AFM scans added to a recipe. Note the inset red square focusing on the user-toggled ability to save and, more importantly, load a previously generated method such as one acquired from initial survey scans conducted with Park

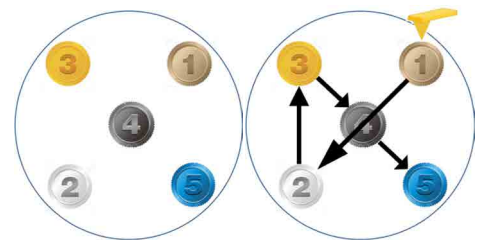
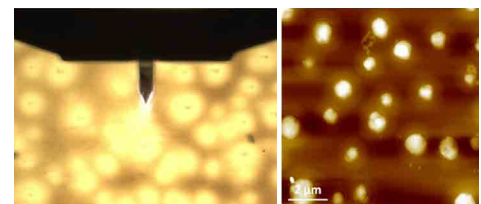


Figure 4. Diagram showing (a) the samples' distribution on the Park NX20's motorized sample stage and (b) the StepScan autocript's -created path the stage took to bring each sample to the AFM probe tip for scanning. The five samples were (1) a PS-LDPE copolymer standard sample, (2) dehydrated collagen fibrils, (3) celgard, (4) an aluminum triangular production pattern, and (5) an SRAM device.



(a)

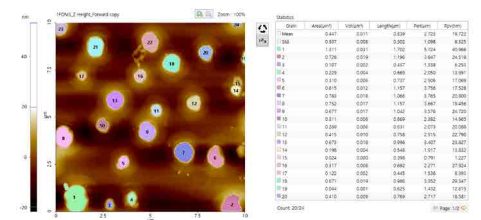


Figure 5. Optical (a) and AFM topography (b) images of the PS-LDPE copolymer standard sample as scanned using StepScan autocript mode. (c) "Grain analysis" as performed with the image processing software Park XEI based on customized criteria to determine the areas of each LDPE cluster. Scan size: 10  $\mu\text{m}$   $\times$  10  $\mu\text{m}$ , image size: 256 px  $\times$  256 px.

Using the “Grain” function of a separate piece of image processing software, Park XEI, it was determined that the mean area of the LDPE clusters was roughly  $0.447 \mu\text{m}^2$ .

### Collagen fibrils

Figure 6 exhibits the optical (a) and AFM topography (b) images of dehydrated collagen fibrils. Collagen is an important structural protein most commonly found in the form of very long fibrils with an axial periodic structure and is abundant in animal tissues [6]. The AFM image unambiguously reveals the differences between the fibrils and the substrate on which they were mounted. Each fibril is revealed to be segmented upon closer inspection of its topography. Furthermore, the fibrils were observed to be gathered in several bundles whose diameters ranged from 60 to 600 nm depending on the number of constituent bodies.

### Celgard

Figure 7 consists of the optical (a) and AFM topography (b) images of the Celgard sample. The AFM image provides evidence of Celgard having a porous and height-varied structure as well as the presence of freely suspended fibril-like structures—both of these features would prove challenging to track with other microscopy techniques. The sample height variation detected is about 60 nm. As observed below, celgard’s otherwise difficult to characterize surface topography was not a problem for non-contact AFM imaging via StepScan autoscript.

### Aluminum triangular production pattern

Figure 8 displays the (a) optical and (b) AFM topography images of the aluminum triangular production pattern sample. This sample is noteworthy because it features sharp edges as tall as 15 nm. Fully formed triangles on the sample were found to be equilateral in geometry and featured side lengths of 170 nm. The self-optimized scan parameters obtained in the initial Auto Mode survey scan remained viable when used in a later scan on the same sample after the AFM had been scripted to image other types of samples in the interim period.

### SRAM device

Figure 9 consists of the (a) optical, (b) AFM topography, and (c) 3D AFM topography images of the final sample: an SRAM

device. SRAM is one of the major types of computer memory and is a common candidate for nanoscale characterization studies [7]. The height variation on this sample is even greater than that of the aluminum triangular production pattern as the device trenches were a steep 400 nm drop from the top of the device. This particular sample was imaged at a higher scan speed than the other samples in the set and is noteworthy for the AFM images’ quality despite this condition.

### Summary

Autoscript, along with other user productivity initiatives introduced by Park Systems, represents a sea change in how much work an AFM can accomplish. The sweeping increase in AFM throughput generated by Autoscript is not limited to veteran users already intimately familiar with how best to scan particular types of samples. Beginner AFM users, as well as those who are working with unfamiliar samples, are now just as capable as more experienced colleagues of acquiring the highest resolution and most accurate images from multiple (and even completely dissimilar) samples en masse. Opening up the power of AFM to a wider audience, democratizing the technology by making its more compelling features more accessible than ever before, is one of the key motivations that drove the development of the Autoscript function and the rest of Park SmartScan operation software. The proliferation of nanoscale characterization via AFM and the corresponding increase in the volume and quality of nanoscience research are now merely matters of time and adoption.

### References

- [1] Park SmartScan – Park Systems. Retrieved October 07, 2016, from <http://www.parkafm.com/index.php/products/operating-software/park-smartscan>
- [2] Park NX20 AFM Options – Park Systems. Retrieved October 07, 2016, from <http://www.parkafm.com/index.php/products/large-sample-afm/park-nx20/specifications>
- [3] Park NX20 – Park Systems. Retrieved October 07, 2016, from <http://www.parkafm.com/index.php/products/large-sample-afm/park-nx20/>
- [4] PPP-NCHR – NANOSENSORS. Retrieved October 07, 2016, from <http://www.nanosensors.com/PointProbe-Plus-Non-Contact-Tapping-Mode-High-Resonance-Frequency-Reflex-Coating-afm-tip-PPP-NCHR>
- [5] Ryu, J.G., Kim, H., Kim, M.H., and Lee, J.W., Morphology and mechanical properties of LDPE/PS blends prepared by ultrasound-assisted melt mixing, Korea-Australia Rheology Journal, September 2004, vol. 16, no. 3, pp. 147-152.
- [6] Kadler, K.E., Holmes, D.F., Trotter, J.A., and Chapman, J.A., Collagen fibril formation, Journal of Biochemistry, May 1996, vol. 316, pp. 1-11.
- [7] Pineda, J.P., Pascual, G., Kim, B., and Lee, K., Electrical Characterization of Semiconductor Device Using SCM and SKPM Imaging, NanoScientific, 2016, Fall, pp.14-16.

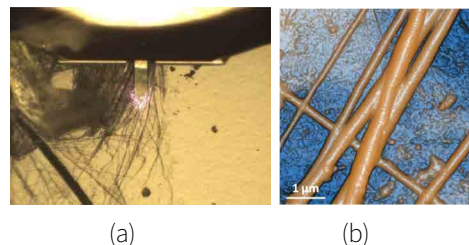


Figure 6. Optical (a) and AFM topography (b) images of the dehydrated collagen fibrils sample as scanned using StepScan autoscript mode. Scan size:  $5 \mu\text{m} \times 5 \mu\text{m}$ , image size:  $256 \text{ px} \times 256 \text{ px}$ .

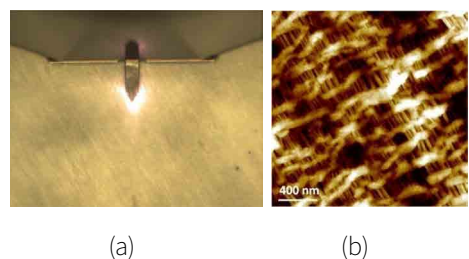


Figure 7. Optical (a) and AFM topography (b) images of the celgard sample as scanned using StepScan autoscript. Scan size:  $2 \mu\text{m} \times 2 \mu\text{m}$ , image size:  $256 \text{ px} \times 256 \text{ px}$ .

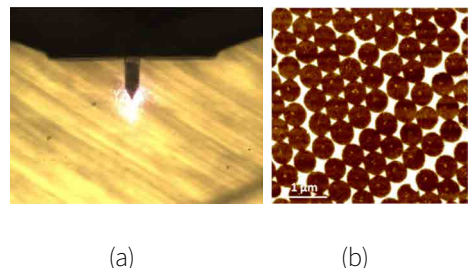


Figure 8. Optical (a) and AFM topography (b) images of the aluminum triangular production pattern sample as scanned using StepScan autoscript mode. The sides of each of the completed triangles are 170 nm each in length. Scan size:  $2 \mu\text{m} \times 2 \mu\text{m}$ , image size:  $256 \text{ px} \times 256 \text{ px}$ .

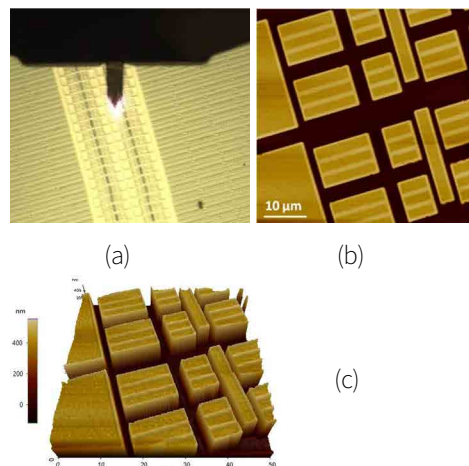


Figure 9. Optical (a), AFM topography (b), and (c) 3D AFM topography images of the SRAM device sample as scanned using StepScan autoscript. Scan size:  $50 \mu\text{m} \times 50 \mu\text{m}$ , image size:  $256 \text{ px} \times 256 \text{ px}$ .

# NANOSCIENCE IN GEOSCIENCE – NANOPORE CHARACTERIZATION USING ATOMIC FORCE MICROSCOPE

Farzam Javadpour, Ph.D.

Bureau of Economic Geology, Jackson School of Geosciences, The University of Texas at Austin



Geoscience is a branch of science dealing with the physical and chemical constitution of the Earth and its atmosphere. Nanoscience is the study of structures and materials on the scale of nanometers. To give you an idea of how small a nanometer (nm) is, a string of hair is about 75,000 nm in diameter and a human red blood cells is about 7,000 nm. Structures at the nanometer scale take on fascinating properties that are normally ignored at larger scale. One intriguing nanostructure present in geological systems is the existence of nanoscale pores—nanopores—in underground shale gas and tight oil reservoirs. These deep geological formations host enormous stores of oil and gas generated over millions of years. Many of these nanopores are interconnected in shale gas and tight oil reservoirs.

These tight reservoirs can produce both natural gas and oil thanks to horizontal drilling and multistage hydraulic fracturing technology. The Darcy equation is a well-accepted equation relating pressure gradient to flux in porous media. In the past few decades, the oil industry has successfully used the Darcy equation for conventional oil and

gas reservoirs, which have pores ranging from 10 micrometers to hundreds of micrometers—orders of magnitude larger than the nanopores in shale and tight oil reservoirs. The small size of nanopores makes the Darcy equation inaccurate for modeling gas and liquid flow in such tight systems.

We study and model the transport of water, gas, and oil in shale and tight oil reservoirs. Our research has immediate applications in hydraulic fracturing design to optimize fracture-to-fracture spacing and well-to-well spacing. Optimizing the separation space between fractures and wells reduces the cost per barrel, making the development of these strata economically and environmentally feasible. Gas-flow models and oil-flow models are also needed to assess in-place gas and oil, production deliverability, and further production optimization in these reservoirs.

## Detecting Nanopores

Pores size and connectivity are important features of any porous material. The mean pore size in conventional oil and gas reservoirs ranges from

10 micrometers to hundreds of micrometers, whereas in unconventional shale gas and tight oil reservoirs, the mean pore size is three orders of magnitude smaller—10 nanometers to hundreds of nanometers. There are two major methods for detecting pores in porous samples: (1) direct pore detection through visualization and (2) indirect methods such as capillary pressure tests using mercury injections [1-2]. Both direct and indirect methods have their own pros and cons. Direct methods can reveal pore geometries and their location among many different mineral types but are limited to a two-dimensional planar view and location. Indirect methods provide pore size distribution for the entire sample in three dimensions but lack information about pore geometry and location. Indirect methods are generally more expensive, time consuming, and sometimes destroy the sample, limiting additional testing on the same sample.

Light microscopes have been used to examine thin sections of the rock samples and directly visualize pores in conventional reservoirs. However, the small size of the nanopores in shale gas and tight oil reservoirs make it necessary to use other imaging methods for these samples. Scanning electron microscopy (SEM) [3] and atomic force microscopy (AFM) [4] have recently been used. Both SEM and AFM can detect pores at the nanoscale if a sample with a perfectly flat surface is available.

The study of pore systems in shales took a major leap forward with the introduction of Ar-ion milling as a sample preparation technique to provide a flat sample surface [5]. Examination of Ar-ion-milled surfaces using high-

field-emission SEM has made it possible to define different pore types on the scale of micro- to nanometers (interparticle, intraparticle, and organic matter) which are common to shales [6]. In particular, numerous types of pores were shown to be developed in different varieties of organic matter (kerogen, bitumen, and pyrobitumen) [7].

One of the early concerns of the SEM technique for detecting nanopores in shale samples was whether the detected nanopores were truly natural pores or in fact the result of high-energy beam emission during SEM imaging. This concern was especially critical because most nanopores were detected in organic materials (Fig. 1), which are possibly sensitive to high-energy beams. Therefore, although SEM detection of these pores was an exciting and an important development, a second method was needed to validate the existence of nanopores in shale. We used atomic force microscopy (AFM) to detect the nanopores and confirm that many of the nanopores detected by SEM occurred naturally [4].

An atomic force microscope—one of a family of scanning probe microscopes widely used to study biological systems and material science—can directly measure the interactive forces between surfaces or molecules. AFM can be used to measure the topography of surfaces and examine the geometry and size of pores at the nanoscale. It can also be used to measure surface forces such as van der Waals (vdW) and the electrostatic forces between molecules of interest and mineral rocks.

AFM uses a flexible cantilever which acts as a spring to determine the net force between a coating at the tip of the cantilever and a sample. Local attractive and repulsive forces between the tip and the sample material basically bend the cantilever arm. The proximal end of the cantilever is attached to a rigid base that allows vertical movement with piezoelectric materials (Fig. 2). The movement of the cantilever is detected and converted into an electrical signal to produce force curves versus distance. The detection system that has become the standard uses a focused laser beam that is reflected from the rear of the cantilever onto a detector. Using the optical lever principle, a

small displacement of the cantilever is converted into a measurably large deflection in the position of the reflected spot on a photodetector (Fig. 2).

Most atomic force microscopes use a photodiode divided into four quadrants, which enables the localized laser spot to be determined in two dimensions. Signals from these four quadrants are compared to determine the deflection signal. Vertical deflection can be calculated by comparing the spot location between the top and bottom halves of the detector. Lateral twisting of the cantilever can also be calculated by comparing the spot location on the left and right halves of the detector. Figure 3 shows the surface topography of a  $4.0 \times 4.0 \times 0.6\text{-}\mu\text{m}$  area of a shale sample measured with AFM. It is one of the first AFM images of a shale sample scanned in the NanoGeosciences Laboratory at the Bureau of Economic Geology (Jackson School of Geosciences, The University of Texas at Austin).

Detecting pores and determining their connectivity helps us to understand the movement of different fluid molecules through porous strata and to determine permeability. Permeability [8] is a useful macroscopic parameter that tells us how much of the in situ oil and gas is recoverable. It is a critical parameter to helping companies assess plays for investment and budget for development. It can be used in many field applications such as designing processes for hydraulic fracturing. Hydraulic fracturing is an expensive process that uses huge amount of water; therefore, any improvement in the accuracy of its application is environmentally and economically attractive.

In addition to using AFM to detect nanopores on surfaces, we also use AFM to measure force spectroscopy between fluid molecules and pore wall materials. These measurements are necessary to determine parameters such as liquid slip length in liquid-flow models. In the next section, we present brief discussions on gas and liquid flow in the nanopores of shale gas and tight oil reservoirs. Later, we describe the digital techniques used to generate three-dimensional digital models of shale to determine permeability. We conclude by discussing the application of these measurements and modeling efforts in hydraulic

fracturing design and production forecast models necessary for field investment and development.

### Single-Phase Gas Flow Model

Gas flow in nanopores deviates from the Darcy equation through the life of a well in shale gas reservoirs. Early in a well's life, when the reservoir pressure is high, gas flow may follow the Darcy equation; however, when reservoir pressure is declined, it may deviate from Darcy equation. The Knudsen number is a criterion that can be used to determine whether the Darcy equation is valid:

$$K_n = \lambda/d \quad (\text{Eq. 1})$$

$$\lambda = (k_B T) / (\sqrt{2} \pi \delta^2 P) \quad (\text{Eq. 2})$$

In which  $\lambda$  is mean free path,  $d$  is average pore size,  $k_B$  is the Boltzmann constant,  $\delta$  is gas molecule size, and  $T$  and  $P$  are temperature and pressure, respectively. Figure 4 shows different flow regimes as a function of the Knudsen number and the validity of the Darcy equation as a function of the Knudsen number.

Javadpour (2009) [8] proposed superimposing Brown's gas-slip flow and Knudsen diffusion to create a general form of gas-flow model for shale gas reservoirs. This is possible because these two processes may not act simultaneously during the life of a well. Early in the life of a reservoir (or well) pressure is high and Knudsen diffusion is negligible, so it is possible for gas slip to be the dominant process, even for systems with extremely small pores. Gas-slip dominance continues until pressure drops below about 600 psi. At 600 psi, operators usually abandon the well. So, in practice, gas slip is the main contributing process in the field. Although shale reservoirs do not operate at pressures lower than 600 psi, modeling gas flow at lower pressures is necessary for bench experimentation, e.g., GRI and pulse-decay permeability tests [9]. It is easier to run tests at low pressures, and the proposed model can then be used to correct the experimental permeability data for the Knudsen diffusion effects.

The most recent models are built upon the earlier model with some modifications to account for the flow of real gas in porous media and surface roughness [10-13].

An easy way to show the difference between the Darcy permeability model and our proposed model—hereinafter called apparent permeability—is to plot the ratio of apparent permeability to Darcy permeability. The ratio of apparent permeability ( $k_{app}$ ) to Darcy permeability ( $k_D$ ) for the models proposed is given by Equation 3:

$$\frac{k_{app,pm}}{k_D} = \frac{\mu M}{RT \rho_{avg}} \frac{\phi}{\tau} (\delta')^{D_f-2} \frac{D_k}{k_D} + \left(1 + \frac{b}{p_m}\right)$$

$$b = \left(\frac{8\pi RT}{M}\right)^{0.5} \frac{\mu}{r} \left(\frac{2}{\alpha} - 1\right) \quad (\text{Eq. 3})$$

in which  $\mu$ ,  $M$ , and  $\rho$  are viscosity, molar mass, and density of gas at average reservoir pressure  $p_m$ , respectively.  $R$  is the gas constant,  $T$  is absolute temperature,  $r$  is average pore size,  $\phi$  is porosity,  $\tau$  is tortuosity,  $D_f$  is fractal dimension,  $\delta'$  is the ratio of normalized gas molecule size to local average pore size, and  $\alpha$  is the tangential momentum accommodation coefficient (TMAC). Equation 3 shows that permeability is pressure-dependent, assuming Knudsen diffusion and slip flow (the “Klinkenberg effect”) are the main mechanisms of the overall flow in shale gas reservoirs. Figure 5 shows apparent permeability as a function of pressure in a shale system with different average pore sizes. The TMAC is the only parameter in Equation 3 that was not readily available for shale samples. TMAC depends on gas molecule type and the material of the pore wall. Singh and Javadpour (2015) [11] developed a method to determine TMAC from gas desorption tests conducted on shale samples. Gas desorption is a routine test that most companies run on their shale samples.

### Single-Phase Liquid Flow Model

The leak-off of hydraulic fracturing fluid into the matrix and the production of oil and water from shale gas and tight oil reservoirs are examples of liquid transport in these systems. In most engineering applications, it is valid to assume no-slip boundary conditions; however, when dealing with nanopores, liquid slippage on pore walls is not negligible and needs to be included in flow models [14]. Various authors have come up with diverse ways of estimating liquid slippage based on theoretical [15-16] and semi-empirical models [16-17]. Recently, molecular

dynamics simulations [18-19] and lattice Boltzmann methods [20] have also been used to study liquid flow in nanoporous shale and tight oil systems. We developed an AFM metrology to measure liquid slip length for the leakoff of fracturing fluid in shale-gas and tight-oil reservoirs [14]. Please note that although gas slippage and liquid slippage are similar processes for describing gas and liquid slippage in pores, the methods to determine gas slippage and liquid slippage are different.

Liquid slip length depends on fluid type, pore-wall material, and flow rate. Vinogradova (1995) [21] made a theoretical study of the drainage of a thin liquid film between two undeformable surfaces. She suggested that the slippage is probably linked to the decrease in viscosity of the thin layer near the wall. Under equivalent conditions, the liquid slip length within a pore and over an object (e.g., a spherical particle) is the same. However, measuring liquid slip length over an object is easier. Therefore, we use spherical particles and flat substrate of a similar material to the pores in shale to measure liquid slip length. The measured liquid slip length will be used in digital shale models to determine effective liquid permeability corrected for the liquid slip length.

The force acting on a sphere with radius  $R_1$  approaching another sphere with radius  $R_2$  is defined as:

$$F = (6\pi R_e^2 \mu v) / h f^* \quad (4)$$

$$R_e = (R_1 R_2) / (R_1 + R_2) \quad (5)$$

in which  $h$  is the separation distance between the surfaces of two hydrophobic spheres and  $f^*$  is the slippage correction factor for approaching spheres, with relative velocity of  $v$  in a liquid with viscosity  $\mu$ .<sup>21</sup>

$$f^* = h/3b [(1+h/6b)\ln(1+6b/h)-1] \quad (6)$$

For the limiting case of  $R_2 \rightarrow \infty$ ,  $R_e \rightarrow R_1$ , the solution can be used for a hydrophobic sphere approaching a hydrophobic flat surface.

Figure 6 illustrates an AFM setup with a spherical particle attached to the cantilever that approaches a flat substrate. Cantilever deflection versus separation distance between the particle

and the substrate was measured and later converted into acting force on the particle as a function of separation distance using Hooke’s law (Fig. 7). Liquid slip length can be determined by fitting Equation 6 to force-distance experimental data.

### Digital Realization of Nanoporous Shale

Direct measurement of permeability in shale and tight oil samples is not an easy task. Current measuring techniques are expensive, time-consuming, and still evolving. We use digital realizations as an alternate approach to obtaining permeability values from more reliable and readily available measuring data such as porosity, pore-size distribution, and mineralogy [22]. In addition, permeability in shale is not only a rock characteristic; it also depends on fluid types, pressure, temperature, and pressure gradient. Therefore, a model that predicts different fluid type (oil, gas, water) and different pressure and pressure gradient conditions can save time and costs.

Characterization of shale samples, which are typically low permeability, is very difficult due to the presence of multiscale structures. Though three-dimensional (3D) imaging can be an ultimate solution for revealing important complexities of such samples, acquiring these images is impractical due to the cost and processing time. On the other hand, high-quality two-dimensional (2D) images, which are widely available, also reveal useful information about organic-matter distribution, associated pores in organic and inorganic matter, and pore connectivity. The objective is to construct 3D digital images from 2D SEM or AFM images and then perform fluid-flow modeling to gain understanding of fluid flow and permeability in 3D blocks of shale samples. We have used different reconstruction approaches, such as image-based and object-based models (Fig. 8), to determine effective gas and liquid permeability in shale and tight oil systems [23-26]. The resultant effective gas and liquid permeability can then be used in fluid-flow simulations or hydraulic-fracturing design.

### Application to Hydraulic Fracturing

The distance between horizontal wells and the separation distance between

aspects of any unconventional shale gas or tight oil reservoir development (Fig. 9). The reservoir becomes overstimulated if the wells are too close to each other or if the separation distance between fracturing stages is too close. Overstimulation is costly and increases the cost per barrel. However, if the wells are too far apart or the hydraulic-fracturing separation distance is too far, then a significant portion of the reservoir remains unstimulated, which also increases the cost per barrel. Effective liquid permeability is needed to optimize hydraulic-fracturing design in terms of well-to-well distance and fracture-to-fracture-distance.

Figure 10 highlights the importance of effective liquid permeability on hydraulic-fracturing design. Underestimated liquid permeability results in overestimation of induced fracture networks. Hence, wells will be drilled too far apart, and the fracture spacing between fracture stages will also be too far apart [14]. A proper fracturing design is cost effective with minimum environmental impacts.

### Application to Production Decline Forecasts

Matrix permeability, the network of induced fractures, and their properties control pressure propagation and fluid flow in hydraulically fractured shale and tight oil reservoirs. We developed a novel, fully fractal model in which both the spacing and the porosity/permeability of induced fractures are distributed based on fractal dimensions, i.e., fractal decay of fracture density and the associated porosity/permeability away from the main induced fracture [27]. The fractal fracture distribution is general—that is, it handles exponential, linear, power, and uniform distributions. We also developed a new, fully fractal diffusivity equation based on the fractal distribution of fractures and their properties. Then, for the first time, we used the semianalytic Bessel spline scheme to solve the developed diffusivity equation.

Our proposed model [27] is general and can capture any form of induced-fracture distribution for better analysis of pressure response and production rates at transient and pseudo-steady-state conditions. We used these models

to match and predict production data from a multifractal horizontal gas well in the Barnett Shale (Fig. 11). Our results showed the importance of estimated matrix permeability to improve matching field data.

### References

- (1) Javadpour, F.; Fisher, D.; Unsworth, M., Nano-scale Gas flow in shale sediments. *Journal of Canadian Petroleum Technology* 2007, 46(10), 55–61.
- (2) Wang, S.; Javadpour, F.; Qihong, F., Confinement Correction to Mercury Intrusion Capillary Pressure of Shale Nanopores. *Scientific Reports* 2016, Feb. 1, 6:20160, 1–11.
- (3) Reed, R. M.; Sivil, J. E.; Sun, X.; Ruppel, S. C., Heterogeneity of Microscale Lithology and Pore Systems in an Upper Cretaceous Eagle Ford Group Horizontal Core, South Texas, USA. *GCAGS Journal* 2019, 8, 22–34.
- (4) Javadpour, F.; Moravvej, M.; Amrein, M., Atomic Force Microscopy (AFM) A New Tool for Gas Shale Characterization. *Journal of Canadian Petroleum Technology* 2012, 51(4), 236–243.
- (5) Loucks, R. G.; Reed, R. M.; Ruppel, S. C.; Jarvie, D. M., Morphology, Genesis, and Distribution of Nanometer-scale Pores in Siliceous Mudstones of the Mississippian Barnett Shale: *Journal of Sedimentary Research* 2009, 79, 848–861.
- (6) Loucks, R. G.; Reed, R. M.; Ruppel, S. C.; Hammes, U., Spectrum of Pore Types and Networks in Mudrocks and a Descriptive Classification for Matrix-related Mudrock Pores. *American Association of Petroleum Geologists Bulletin* 2012, 96(6), 1071–1098.
- (7) Reed, R. M.; Loucks, R. G.; Ko, L. T., Scanning Electron Microscope Petrographic Differentiation among Different Types of Pores Associated with Organic Matter in Mudrocks. *GCAGS Journal* 2020, v. 9. To appear in October issue.
- (8) Javadpour, F., Nanopores and Apparent Permeability of Gas Flow in Mudrocks (Shales and Siltstone). *Journal of Canadian Petroleum Technology* 2009, 48 (8), 16–21.
- (9) Javadpour, F.; Etehadavakkoli, A., 2015, Book chapter, Chapter 11: Fluid Flow Processes in Shales. (Book: *Fundamentals of Gas Shale Reservoirs*; Editor: Reza Rezaee, Publisher: John Wiley and Sons Inc., ISBN 9781-118-64579-6 hardback).
- (10) Darabi, H.; Etehad, A.; Javadpour, F.; Sepehrnoori, K., Gas Flow in Ultra-tight Shale Strata. *Journal of Fluid Mechanics* 2012, 710, 641–658.
- (11) Singh, H.; Javadpour, F., Langmuir Slip-Langmuir Sorption Permeability Model of Shale. *Fuel* 2015, 164, 28–37.
- (12) Afsharpoor, A.; Javadpour, F., Liquid Slip Flow in a Network of Shale Noncircular Nanopores. *Fuel* 2016, 180, 580–590.
- (13) Wang, S.; Qihong F.; Javadpour, F.; Zha, M.; Cui, R., Multiscale Modeling of Shale Apparent Permeability: An Integrated Study of Molecular Dynamics and Rigid Pore Network Model. *SPE Journal* 2020. Available online.
- (14) Javadpour, F.; McClure, M.; Naraghi, M.E., Slip-corrected Liquid Permeability and its Effect on Hydraulic Fracturing and Fluid Loss in Shale. *Fuel* 2015, 160, 549–559.
- (15) Philip J. R., Flows Satisfying Mixed No-slip and No-shear Conditions. *Zeitschrift für angewandte Mathematik und Physik* 1972, 23, 353–372.
- (16) Lauga E; Stone H., Effective Slip in Pressure Driven Stokes Flow. *Journal of Fluid Mechanics* 2003, 489, 55–77.
- (17) Ou J.; Perot B.; Rothstein J. P., Laminar Drag Reduction in Micro Channels Using Ultrahydrophobic surfaces. *Physics of Fluids* 2004, 16(12), 4635–4643.
- (18) Wang, S.; Javadpour, F.; Qihong, F., Fast Mass Transport of Oil and Supercritical Carbon Dioxide Through Organic Nanopores in Shale. *Fuel* 2016, 181, 741–758.
- (19) Wang, S.; Javadpour, F.; Qihong, F., Molecular Dynamics Simulation of Oil Transport Through Inorganic Nanopores of Shale. *Fuel* 2016, 171, 74–86.
- (20) Zhang, T.; Javadpour, F.; Yin, Y.; Li, X., Upscaling Water Flow in Composite Nanoporous Shale Matrix Using Lattice Boltzmann Method. *Water Resources Research* 2020. DOI:10.1029/2019WR026007. Available online.
- (21) Vinogradova, O.I., Drainage of a Thin Liquid Film Confined between Hydrophobic Surfaces. *Langmuir* 1995, 11, 2213–2220.
- (22) Naraghi, M.E.; Javadpour, F.; Ko, T.K., An Object-based Shale Permeability Model: Non-Darcy Gas Flow, Sorption, and Surface Diffusion Effects. *Transport in Porous Media* 2018, 125, 23–39.
- (23) Tahmasebi, P.; Javadpour, F.; Sahimi, M., Multiscale and Multiresolution Modeling of Shales and their Flow and Morphological Properties. *Scientific Reports* 2015a, 5:16373, 1–11.
- (24) Tahmasebi, P.; Javadpour, F.; Sahimi, M., Three Dimensional Stochastic Characterization of Shale SEM Images. *Transport in Porous Media* 2015b, 110, 521–531.
- (25) Tahmasebi, P.; Javadpour, F.; Sahimi, M., Multiscale Study for Stochastic Characterization of Shale Samples. *Advances in Water Resources* 2016a, 89, 91–103.
- (26) Tahmasebi, P.; Javadpour, F.; Sahimi, M., Stochastic Shale Permeability Matching: Three-Dimensional Characterization and Modeling. *International Journal of Coal Geology* 2016b, 165, 231–242.
- (27) Sheng, G.; Javadpour, F.; Su, Y.; Liu, J.; Li, K.; Wang, W., A Semianalytic Solution for Temporal Pressure and Production



### Biography

Farzam Javadpour holds B.Sc. with distinction in petroleum engineering, and M.Sc. & Ph.D. degrees in chemical and petroleum engineering from the University of Calgary (Canada). Javadpour has worked as a reservoir engineer in industry and is currently working as a Research Scientist at the Bureau of Economic Geology (Jackson School of Geosciences, University of Texas at Austin). Javadpour is the CO-PI of Mudrock Systems Research Laboratory (MSRL) consortium and leads research works on novel techniques of reserve and permeability estimations as well as oil and gas production in mudrock/shale systems. Javadpour is also studying fundamentals of nanoparticle transport in porous media for EOR and reservoir-engineering applications. Javadpour teaches shale-gas characterization and production at the University of Texas at Austin. Javadpour has published 60 peer-reviewed journal papers and 25 SPE conference proceedings on topics related to shale gas, CO<sub>2</sub> injection, and transport in porous media. Javadpour's work on the development of apparent permeability formulation for shale-gas systems appeared as a Distinguished Author publication in *Journal of Canadian Petroleum Technology* (JCPT-2009). Javadpour served as associate editor for (JCPT) and was the recipient of the award for the best paper published in JCPT in 2008, the SPE "Outstanding Service Award" in 2010, and the SPE "A Peer Apart Achievement Award" in 2014. Javadpour is currently serving as associate editor of the *SPE Journal*.

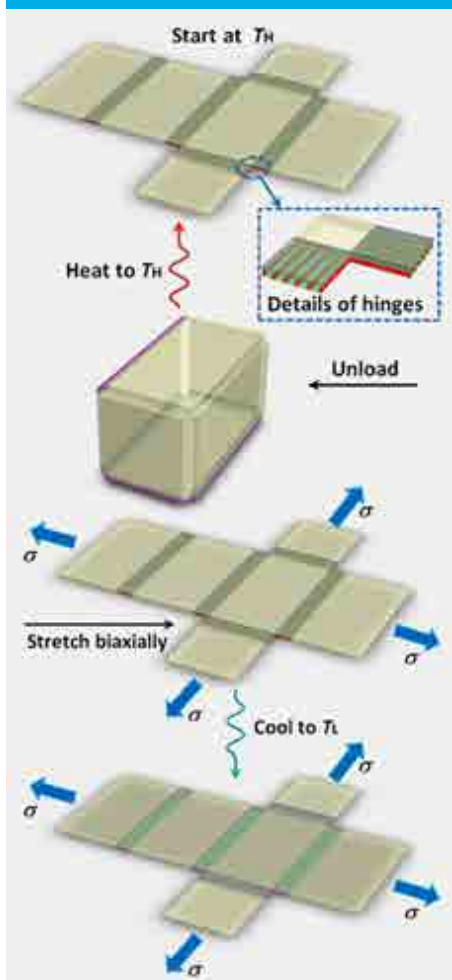
## 4D PRINTING AND STIMULI RESPONSE

### MATERIALS MATTER

Column Highlighting Topics Presented in Dr. Advincula's Monthly Webinars on Advancements in Material Science



## Dr. Rigoberto Advincula, Professor, Macromolecular Science & Engineering, Case Western Reserve University



needs, it is important that more materials become available and more types of new applications are envisioned. This includes adding the fourth dimension of stimuli responses to 3D printed materials.

### What are stimuli responsive materials?

Stimuli responsive materials or polymers are what can be found in micelles, nanogels, and oil and water interfaces – that have the ability to change in shape or dynamics in the presence of stimuli. What is important to note is that stimuli-responsive materials need to have a field effect – the application of temperature, pressure, electric field, or light field – in order to change or elicit response from the particular stimuli. For example, in the case of polymers, we can define them at the nano to microscopic level such that we can control their swelling behavior, their contraction, their micellization, or equilibration at the interface. Types of stimuli that can be applied include temperature, pH, magnetic field, mechanical field, etc. In turn this will elicit a response on the polymer that results in a change in shape, mechanical properties, permeability, phase separation, optical and/or electrical properties.

one to make a variety of shapes. A good example is a shape memory nickel alloy – a material that is used for stents – good for different types of designs or cylinders that can control flow behavior. Many types of materials have been explored including metals and polymers, but in my research, I have been most interested in soft matter or polymer materials.

### How are polymeric materials used in 4D Printing?

So, I mentioned our group is focused on polymeric materials. In particular we have done a lot of work on polymers at interfaces or the chemistry of interfaces and interfacial phenomena. We have done a lot of work on grafting polymers on surfaces or polymer brushes, which can be grafted using control initiators as well as the patterning of different types of polymers. Another specialty in our group is to work on poly-electrolyte multilayers. These electrostatically absorb or equilibrate polymer materials that can be used to lay flat on surfaces or take the shape of the particle or even a route toward hollow shell particles.

### Can you give an example?

A very simple concept is the 3D printing origami approach, using a Japanese-inspired design. The question is – how can you 3D print an object or a precursor object such that you can control the folding in the presence of stimuli? And this can be done, for example, in an origami approach by producing the creases and folds at specific locations on a flat object. The result is that you will have a hinges...you will have a distribution of hinges and folds that

### Where does the future of 3D printing go?

What applications are there in industry, research, biomedical engineering, and even outer space? Common 3D printing methods such as FDM (Fused Deposition Modeling), SLA (Serial Lithographic Apparatus), or SLS (Selective Laser Sintering) are familiar by now and many scientists are actively using them. In order to have as far and as wide an application of 3D printing for industrial and research

### What is 4D Printing?

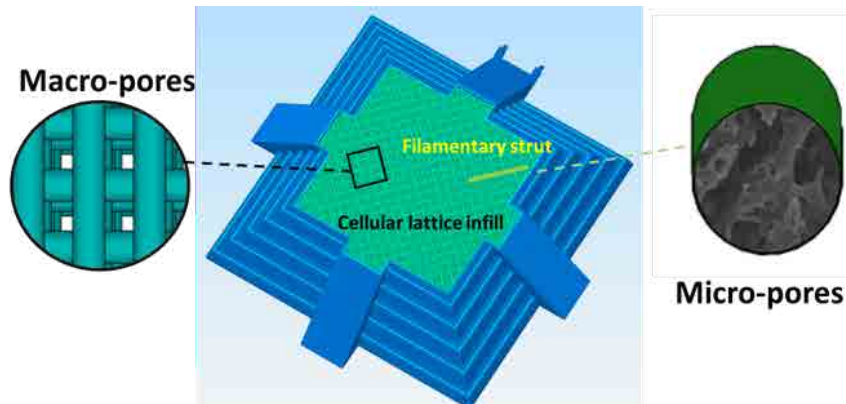
4D printing allows us then to combine the design and materials in order to produce a new effect, some stimuli-response of both the material and the 3D printed object. These methods were first reported by scholars from MIT, who actually coined the term 4D printing, but what this is, simply, is stimuli-response by design. So, 3D printing is extended to “4D,” allowing



Silicon sample image 1 (above). Silicon sample image 2 (below). In this case we use a silicon material, this silicon materials were 3D printed as different objects as shown here with a formulation that shows the amount of PDS and Silicon oil added. The reason is that by varying the amount of silicon oil and salt, we are able to change the porosity.

can be affected and stretched by heat. An advantage of 3D printing is you can actually orient the 3D printing of the material such that you can optimize the mechanical properties as well as the ability to fold.

Many cases have been reported where these architectures can be 3D printed or designed to make very complicated objects out of let's say, a printed or two dimensional design. If you are able to control the placement of those trusses, hinges and corners, with the right material and the right stimuli, when you start folding one side, you will prepare an object that basically has a fourth dimension. 4D that is an outcome of the initially 3D printed design and material as well and other examples of that 2D to 3D to 4D transition. So from flat to three dimensional to 4D, you can convert the access if you design them well, such that without using gears or without using arms, one is able to elicit movement or mechanical movement based on the design.



Soft robotics sample

### What is Shape Memory?

Shape memory means that the original shape can be converted back to with the appropriate stimuli. In other words, when you first form the object, if you maintain that shape, that shape is in the memory of the polymer and you can go back to the original shape as it was formed. Another type of shape memory material is used in stents or different types of biomedical applications. 4D printing the right material or composite material in this case can result in the ability to form folds or structure.

You can essentially program the shape and change them with different combinations of heat or mechanical response such that you can cycle them from one form to the other. This ability to go to various shapes simply means that you have a handle, or several handles, both mechanical and

thermal to change the response. Shape memory material properties are essentially 4D printing because the property is hidden when you first print the object, but then the application of the appropriate stimuli unlocks the property that was originally present during printing.

### Do you have an example from your research?

We were interested in 3D printing different types of origami-like designs, in order to improve the movement of robotic arm methods. Using these principles will be useful for soft robotics or the ability to use 3D printing as a route towards elastomeric or thermoset elastomeric materials that can be used to activate or have movement without the use of gears, arms or different mechanical devices that are currently needed to make robot devices and objects.

### In conclusion...

I hope the readers now have an appreciation of what it means to unlock a property on what we call 4D printing. The combination of design shape with the chemistry or composition of the material itself and the stimuli which you provide, whether heat, electric field, optical field, temperature or otherwise, will elicit a response. Lastly, shape memory is very much applicable to what we can 3D print in objects and metal alloys.

This column is an excerpt from a webinar led by Dr. Advincula describing different types of 3D printed objects and materials that can be manipulated by applying stimuli to become "4D." To listen to the entire webinar, go to: <https://youtu.be/crH-WpS4yE>



**VIRTUAL**

**2020 NanoScientific Symposium**  
For a Changing World

**October 14-15**



**JOIN US!**

# Participate in the poster exhibition and contest!

**CASH PRIZES FOR ACCEPTED ABSTRACTS AND POSTERS!**



You will be Eligible for Cash Awards in excess of \$5,000 and \$100 for Every Poster Accepted

Submit your abstract to be a presenter or display a poster for the poster exhibition by September 30, 2020.

Abstracts and posters should relate to Research in Nanotechnology that improves our changing world. There will be emphasis given to research that includes the use of Scanning Probe Microscopy (SPM), but any scientific category is welcome – medical research, electronics and sensors, chemistry, bioengineering, nanoscale design and other advanced scientific research.

**Submit today to join our exciting program**

Top submissions will be published in an upcoming issue of NanoScientific Magazine!

**Apply at [parksystems.com/nscw](http://parksystems.com/nscw)**

SPONSORED BY



**NANOscientific**

**physicsworld**

